JPL PUBLICATION 82-102

The Deep Space Network — An Instrument for Radio Navigation of Deep Space Probes

N.A. Renzetti
J.F. Jordan
A.L. Berman
J.A. Wackley
T.P. Yunck

December 15, 1982

National Aeronautics and Space Administration

Jet Propulsion Laboratory
California Institute of Technology
Pasadena, California

JPL PUBLICATION 82-102

The Deep Space Network — An Instrument for Radio Navigation of Deep Space Probes

N.A. Renzetti
J.F. Jordan
A.L. Berman
J.A. Wackley
T.P. Yunck

December 15, 1982

National Aeronautics and
Space Administration

Jet Propulsion Laboratory
California Institute of Technology
Pasadena, California

The research described in this publication was carried out by the Jet Propulsion Laboratory, California Institute of Technology, under contract with the National Aeronautics and Space Administration.

PREFACE

In a 1969 publication (Renzetti and Fearey, 1969), we discussed the status of the capability of the Deep Space Network (DSN) to generate observables required for navigating the Mariner class of planetary missions. The radio metric data during that period were primarily 2-way coherent doppler and range between the Earth (Deep Space Stations) and the spacecraft. These data were used by the navigators to compute the trajectory of the spacecraft and provide the basis for trajectory corrections to target the spacecraft to the appropriate distance from the planets. Since that publication, there have been significant improvements in the above data types. In addition, supporting data types such as frequency stability, media calibration (both troposphere and ionosphere effects on the radio signals) and time synchronization between the Deep Space Stations at each of the longitudes were developed and implemented and are currently used for radio navigation. A new data type was also introduced in recent years as a result of the application of radio interferometry at microwave frequencies to the study of compact radio sources. Initially, one station at each complex was instrumented for making observations on extragalactic radio sources and configured as interferometers, with Goldstone/Madrid and Goldstone/Canberra being the inferometer pairs, to provide synchronization of the clocks at each of the complexes. In the processing of these data, we generated values for earth rotation and pole motion. In the next phase, we configured these same stations to make observations both on the spacecraft radio signal and nearby radio sources in order to determine the angle between these two. This data type, generated by the DSN VLBI System MK II-81, is entering the operational phase and is being used by the Voyager Project for targeting the spacecraft to Uranus and thence Neptune. It is also planned to be the primary data type for navigation of the Galileo spacecraft to Jupiter and its satellites.

This report updates the 1969 publication and describes the state-of-the-art capability to navigate by radio to the outer planets as of January 1, 1982.

ACKNOWLEDGEMENTS

The authors would like to thank W. D. Chaney, N. C. Ham, J. P. McDanell, J. I. Molinder, T. Moyer, X. X. Newhall, H. N. Royden, M. G. Roth, O. J. Sovers, E. M. Standish, J. M. Wilcher, M. Tucker, and B. White, all of the Jet Propulsion Laboratory, for their very substantial contributions in bringing this report to fruition.

ABSTRACT

In the National Aeronautics and Space Administration (NASA) deep space program, spacecraft navigation is the process of determining a spacecraft flight path from observations and correcting the flight path to meet mission objectives.

In the 1960's, deep space spacecraft were navigated with Deep Space Network (DSN) generated doppler, which yields the line-of-sight spacecraft velocity. In the late 1960's, the Network added the capability to generate range data. In the 1970's, the Network improved the accuracy of both the DSN doppler and range systems, and augmented navigational capability with hybrid data types such as dual frequency (S- and X-band) downlink doppler and differenced range versus integrated doppler. In the 1980's, heavy reliance is being placed on new navigational data types which have been innovated via Very Long Baseline Interferometry (VLBI) techniques.

This report describes the network configurations used to generate the navigation observables and the basic process of deep space spacecraft navigation at the Jet Propulsion Laboratory (JPL), from data generation through flight path determination and correction. Special emphasis is placed on the DSN Systems which generate the navigation data--the DSN Tracking and VLBI Systems. In addition, auxiliary navigational support functions are described.

TABLE OF CONTENTS

TABLES

FIGURES

I. INTRODUCTION

The Deep Space Network (DSN), managed by the California Institute of Technology-Jet Propulsion Laboratory (JPL) for the National Aeronautics and Space Administration (NASA), is the collection of facilities which communicates with and collects data from spacecraft involved in the exploration of the Solar System. The DSN in 1982 includes major Deep Space Station complexes located approximately 120 degrees around the earth at Goldstone, California; Madrid, Spain; and Canberra, Australia. These stations are connected to a central Network Operations Control Center located in Pasadena and Mission Control Centers at JPL Pasadena as well as various other locations, via a world-wide ground communications facility. Each Deep Space Communications Complex (DSCC) contains one 64-m diameter antenna, one 34-m diameter antenna, and one or more 26-m diameter antennas.[1] The stations are characterized by high-power transmitters, low-noise microwave amplifiers, phase-locked loop receiving systems, and multiple digital data handling subsystems controlled by minicomputers.

The primary functions of the Deep Space Network are:

1. Acquisition of science and engineering ("telemetry") data radiated from spacecraft to Earth at radio frequencies.

2. Transmission of command signals from Earth to spacecraft at radio frequencies.

3. Generation of radio metric (doppler and range), Very Long Baseline Interferometry (VLBI), and calibration data, which are used for navigation of spacecraft and for research into the character and effects of planetary and interplanetary media and forces and geodynamics.

The history of the Network begins in 1958 with the construction of the first Deep Space Station with a 26-m diameter antenna and electronics at 960 MHz, at Goldstone, California, in support of Pioneer III, the first U.S. lunar probe (Renzetti et al., 1961; Renzetti, 1971). In the 1960's, the NASA deep space

[1] The 26-m subnetwork was closed in December, 1981.

program included the Ranger Project to obtain closeup pictures of the moon, the Surveyor Project for lunar landings, and the Lunar Orbiter Project for detailed mapping of the moon; the Mariner Missions with flybys of Venus and Mars, and the Pioneer Missions for exploration of interplanetary fields and particles. Throughout this period, and in response to the requirements levied by these projects, the Network expanded geographically to its current set of complexes, added larger antennas, and greatly increased the technical capabilities of the ground based equipment.

The spacecraft of the 1960's were navigated with DSN generated doppler, which yields the line-of-sight spacecraft velocity. In the late 1960's, the Network added range measurements, to augment doppler navigation.

Throughout the 1970's, increasingly ambitious deep space missions have required more accurate doppler and range measurements, and the Network employed dual frequency (S- and X-band) downlinks and differenced range vs. integrated doppler calibrations to provide the needed accuracy. Hydrogen maser frequency standards were installed to provide precise frequency and timing. The locations of the Deep Space Stations were determined in relation to the planets to within a meter to enhance navigation accuracy.

Missions during this period included the Mariner 9 Mars Orbiter, the Mariner 10 Venus and Mercury flybys, the Pioneer 10 and 11 flybys of Jupiter, the Pioneer 11 flyby of Saturn, the Viking Mars Orbiters and Landers, and the Pioneer Venus Orbiter and Multi-probe Venus atmosphere entry.

The Voyager mission, with its precision encounters with Jupiter and Saturn in 1979, 1980, and 1981, posed the most stringent navigational requirements seen thus far in the history of deep space exploration. These missions employed two-way range measurements obtained nearly simultaneously from two Deep Space Stations, and differenced to remove common error sources, to navigate the spacecraft through the Saturn encounters.

In the late 1980's, the Galileo Mission, with its planned probe of Jupiter's atmosphere and tour of Galilean Satellites, will require even

more precise "differenced" radio metric observables. The Network is therefore developing Very Long Baseline Interferometry (VLBI) techniques to use for the navigation of this important, challenging mission. These same techniques will enable more precise location of the Deep Space Stations from the analysis of Quasar VLBI data.

Organizationally, the Deep Space Network is composed of nine major data oriented systems:

Tracking
Telemetry
Command
Monitor and Control
Test Support
Programming
Radio Science
Very Long Baseline Interferometry
Frequency and Timing

The DSN Tracking System generates the doppler and ranging data types, while the DSN Very Long Baseline Interferometry System generates the VLBI data types.

In the NASA deep space program, navigation (the process of determining the spacecraft flight path from the observations and correcting the flight path to meet a mission's objectives) is performed by the individual flight projects using the data generated at the Deep Space Stations. The Network, in concert with the flight-project-supported navigation facility at JPL, has provided the extremely high accuracy data needed for the outstanding success to date of the planetary exploration program.

This report summarizes the state of Network development in navigation technology and radio metric data systems as of 1982. In Chapter II the Tracking System is functionally described. The performance of this system is described in terms of the accuracy of the products. Chapter III provides a similar summary of the VLBI System. The major elements of the JPL navigation system are detailed in Chapter IV. A description of the

data processing system is presented, and a historical mission-to-mission performance record is provided. Chapter V provides the functional description and performance summary for the key support activities which locate the stations and calibrate the radio metric data.

II. THE DSN TRACKING SYSTEM

A. INTRODUCTION

The DSN Tracking System, one of the nine generic systems of the Network, is comprised of the hardware, software, personnel and procedures required to perform four primary functions:

1. Acquire and maintain the communications link (uplink and downlink) with a spacecraft.

2. Generate radio metric data consisting of doppler, range and angle measurements at each Deep Space Station.

3. Format and transmit the radio metric data to the data users.

4. Perform radio metric data validation to assure that performance requirements are being met.

The radio metric data generated by the Tracking System are used by the various flight project navigation teams for orbit determination, platform parameter determination and ephemeris development. Additionally, the data have numerous radio science applications for celestial mechanics experiments, interplanetary media studies, relativity experiments and gravity wave studies (Renzetti and Berman, 1981). Within the Network, the data are used to monitor the operation of the Tracking System and to validate its performance.

The following subsections provide a functional description of the various subsystems comprising the Tracking System, including a detailed description of the processes involved in generating doppler and range measurements.

B. FUNCTIONAL DESCRIPTION

Elements of the DSN Tracking System are located at both the Deep Space Station (DSS) and the Network Operations Control Center (NOCC). The

subsystems and major assemblies comprising the Tracking System and the data flow between them are illustrated in Figure 1 (Martin, 1977; Ohlson and Reid, 1976; Otoshi, 1975; Renzetti, 1982; Spradlin, 1979a and 1979b; Wackley, 1981).

Using cesium and hydrogen maser timing standards, the Frequency and Timing Subsystem provides highly stable timing pulses and reference frequencies to all the elements of the Tracking System. The Time Formatter Assembly distributes all required frequency and timing with the exception of the 10 pulses per second (pps) signal used by the Metric Data Assembly (MDA) to trigger sampling of the doppler cycle counters.

The generation of doppler and range measurements requires a closed loop from the station to the spacecraft and back to the station. To provide the link from the station to the spacecraft, the Exciter Assembly of the Receiver-Exciter Subsystem generates an S-band ($\sim$2.1 GHz) uplink carrier. The frequency of the carrier, based on predictions supplied by the Network Operations Control Center (NOCC), is the predicted spacecraft receiver best lock frequency appropriately modified to account for the uplink doppler effect. The frequency is synthesized from a Dana model 7010 synthesizer under the control of a JPL constructed Digitally Controlled Oscillator (DCO). This combination of components provides frequency settability of 0.00048 Hz (S-band) and frequency accuracy of $\sim 1.5 \times 10^{-11}$ when tuning. Additionally, the control of the DCO is provided by the Metric Data Assembly (MDA) of the DSS Tracking Subsystem. The carrier is phase modulated with a squarewave ranging signal received from the Planetary Ranging Assembly (PRA) of the DSS Tracking Subsystem (DTK).

The uplink carrier is amplified by the klystron power amplifier of the Transmitter Subsystem to a power level of 20 kW. A capability for amplification to 100 kW is provided at the 64-m DSS, typically for emergency reasons. In order to ensure accurate doppler and range measurements, the transmitter is required to contribute less than 0.2 m phase instability and less than 0.1 m (over 12 hours) group instability to the uplink signal.

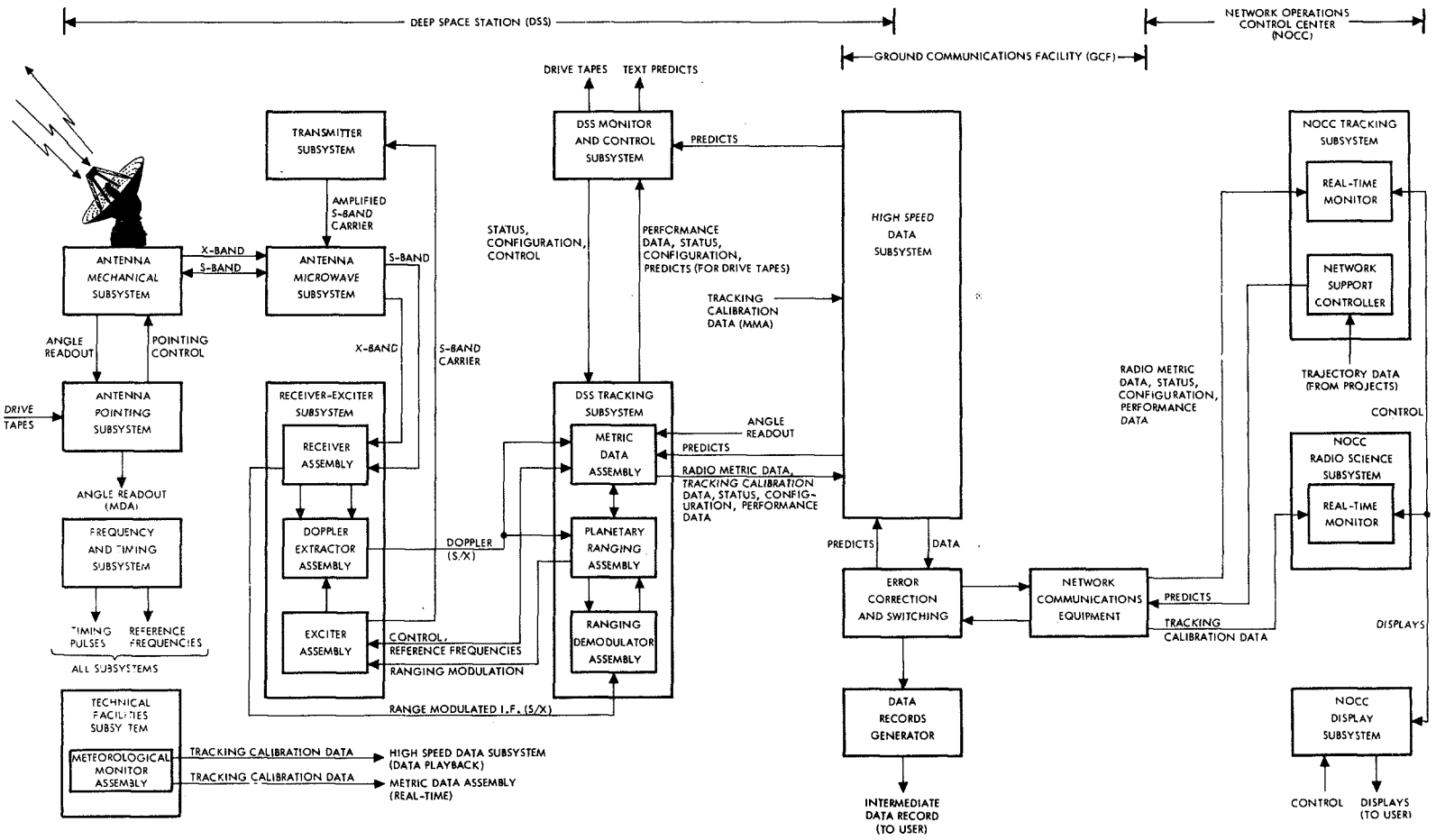

Fig. 1. Tracking System Functional Block Diagram

The amplified signal is provided to the Antenna Microwave Subsystem (UWV) which channels the signal to the antenna for radiation to the spacecraft.

Because of the interplanetary distances involved in deep space communications, it is essential that all possible signal power be received by the spacecraft and ground antennas. To ensure this, the DSN antennas are precisely pointed by the interaction of the Antenna Mechanical Subsystem (ANT) and Antenna Pointing Subsystem (APS). The Antenna Mechanical Subsystem consists of the antenna as well as servomechanical (angle encoders, etc.) and other components required to physically move the antenna. At the 34-m antennas, the current ANT equipment provides positioning accurate to $\pm$ 0.040 degree. At the 64-m antenna, the servo equipment is augmented by the master equatorial which, in essence, converts the AZ/EL antenna to a HA/DEC antenna. This is a more natural reference frame for pointing at celestial type objects and allows for driving the antenna in a constant sidereal rate in hour angle. The pointing accuracy of the 64-m antenna is approximately $\pm$ 0.015 degree.

To improve the pointing of the antenna, a conical scanning (CONSCAN) algorithm has been implemented. This procedure causes the antenna to scan around the predicted position of the spacecraft. By integrating the signal level over the duration of the scan, an angular position offset can be determined and applied to the current position of the antenna.

This method as well as a drive tape, sidereal, manual and planetary (i.e. use of right ascension, declination predicts) drive modes are used by the APS to drive the antenna to follow the radio source.

The antenna focuses the signals received from the Antenna Microwave Subsystem. Using a cassegrain optics arrangement consisting of a hyperbolically shaped primary reflector and a parabolically shaped, steerable (to improve antenna performance) subreflector, the antenna radiates the signal toward the spacecraft.

The spacecraft receives the transmitted signals and demodulates the ranging waveform. The uplink carrier is coherently multiplied (by 240/221 for S-band and 880/221 for X-band) in order to allow for simultaneous

transmission and reception of the signals at the station without interference. The ranging waveform is phase modulated onto the coherent downlink carriers and transmitted back toward the earth.

The downlink carriers at S- and X-band (~8.4 GHz) frequencies are received, focused, and amplified by the antenna and provided to the UWV for further amplification. Using extremely low noise (~5K operating temperature) traveling wave masers, the signal is amplified by ~45 dB. The signal is then provided to the Receiver-Exciter Subsystem.

At the 34-m diameter antenna DSS, the X-band signal is downconverted to S-band by mixing with an appropriately modified exciter reference frequency before being channeled to the Receiver Assembly.

The Receiver-Exciter Subsystem provides phase tracking of the received signal by two types of Receiver Assemblies (the Block III and Block IV Receivers), both of which are triple conversion, superheterodyne, phase-locked loop receivers.

The Block III receiver has been in use by the Network since the mid-1960's with periodic upgrades to improve its performance. This receiver operates in a frequency range of 2270 to 2300 MHz (hence, the required X- to S-band downconversion). It is equipped with 3, 12, 48, and 152 Hz bandwidth Radio Frequency (RF) tracking loop filters to allow tracking under extremely low signal level and/or high doppler rate of change conditions. Additionally, Automatic Gain Control (AGC) loops (with time constants of 4, 34 and 380 seconds) allow for consistent tracking over a wide range of signal level dynamics. Receiver frequency control is provided by a 24 MHz Voltage Controlled Oscillator (VCO) and a Hewlett-Packard frequency synthesizer.

The Block IV Receiver was implemented in the 64-m subnetwork in the early 1970's. It provides for S- or X-band reception (without downconversion) as well as precise, programmable frequency control, using a Programmable Oscillator Control Assembly (POCA) and a Dana Synthesizer. The Block IV Receiver provides improved phase stability and tracking capability. It is equipped with 1, 3, 10, 30, 100 and 300 Hz RF tracking loop filters to

allow for consistent performance over a wide range of doppler and signal level conditions. With AGC loops of time constants of 4, 48, and 480 seconds, the receiver can track signals over a wide range of signal level dynamics.

The Receiver Assembly uses the reference frequency of the phase-locked loop for doppler extraction (see Subsection C) and provides an analog waveform to the MDA (part of the DTK) for counting and to the PRA for use in doppler rate-aiding.

Additionally, a 10 MHz Intermediate Frequency (IF) modulated with the range code is provided to the Ranging Demodulator Assembly (RDA; also part of the DTK) for use in generating ranging data (see Subsection D).

The DSS Tracking Subsystem (DTK), consisting of the Ranging Demodulator Assembly (RDA), the Planetary Ranging Assembly (PRA), and the Metric Data Assembly, is the heart of the Tracking System. The RDA demodulates the range code from the IF. By comparing the range code with a PRA-provided reference code, the RDA generates a series of correlation voltages. The Planetary Ranging Assembly (PRA) generates data based on the correlation voltages generated by the RDA. Addition- ally, the PRA provides the ranging code waveform to the Exciter Assembly for modulation onto the uplink carrier.

The Special Equipment Rack of the MDA provides counters for counting doppler and exciter reference frequencies.

The MDA interfaces with the Digitally Controlled Oscillator (DCO) of the exciter for frequency control. The MDA also provides a capability to construct uplink acquisition tuning sweeps control commands as well as special tuning profiles to allow coherent tracking of the Voyager 2 spacecraft and to calibrate the Voyager 2 receiver.

To provide antenna pointing, the MDA receives angle predictions and provides them to the Digital Instrumentation Assembly for conversion to a (paper) drive tape. Using doppler frequency predictions (included with the angle predictions), the MDA computes doppler pseudo-residuals useful

for validating the doppler data. Additionally the MDA computes parameters useful for validating the ranging data.

The MDA accumulates the doppler and range measurements, validation parameters, reference frequencies, configuration data and status data. It formats these data into 1200-bit data blocks and provides the data blocks to the Communications Monitor and Formatter (CMF) of the Ground Communications Facility (GCF) for transmission to JPL.

Additionally, at the 64-m DSS, the Meteorological Monitor Assembly (MMA) accumulates radio metric calibration data types. Most important of these are measurements of ionospheric electron content (Faraday rotation), which are used to generate ionospheric range and doppler corrections. Also accumulated are measurements of the local weather conditions such as atmospheric pressure, ambient temperature and relative humidity for use in generating tropospheric corrections to doppler and range.

The Faraday rotation angles are generated by continuously tracking linearly polarized VHF downlink signals from one of several (ATS-1, ATS-5, ETS-2, and SIRIO) geostationary satellites and measuring changes in the polarization angle of the signal. The Faraday rotation data thus provides an indirect measure of the electron content along the spacecraft line-of-sight. The data are used for calibrating the ionosphere and providing doppler and range corrections (see Section V).

The MMA provides the data in real time to the MDA for transmission (via GCF) to JPL whenever the DSS is tracking. Additionally, it continuously records the data for weekly transmission to JPL.

The data blocks from the MDA and MMA are received at the GCF Central Communications Terminal (CCT). At the CCT the data are routed via the Error Correction and Switching (ECS) Assembly to the Network Operations Control Center and to the GCF Data Records Generator (DRG). No direct real-time interface exists for supplying the data to the flight project navigation teams. Instead, all data are logged on the DRG disk and periodically (~every 3 days for normal cruise operations but upon request for critical operations), an Intermediate Data Record (IDR) tape of the

data is written and provided to the project. This IDR contains at least 95 percent of the generated radio metric data. During critical phases, the IDR contains at least 98 per cent of the data. The DRG additionally provides a capability to recall data from the station Digital Original Data Record (DODR) should the percentage of missing data exceed allowable limits.

Simultaneously with the DRG reception of data, the radio metric data are routed to the NOCC Tracking Subsystem (NTK) and the real-time tracking calibration data are routed to the NOCC Radio Science Subsystem (NRS). The NRS consists of a Real-Time Monitor (RTM) Assembly (Modcomp II computer) which provides displays of the Faraday rotation data in near-real time. The NTK consists of a RTM (also a Modcomp II computer) and of software resident on the NOCC Support Subsystem (NSS). The RTM receives and processes the radio metric data. Digital Television (DTV) displays of the data are generated and provided to the Network Analysis Team and the Network Operations Control Team via the NOCC Display Subsystem (NDS). The displays are used for real-time monitoring of system performance and data quality. Since these displays provide the only near-real-time observations of the radio metric data, they are made available to navigation personnel.

The NSS consists of the Network Support Controller Assemblies (NSC). The NSC are a pair of identically configured Xerox Sigma 5 computers with 64K words of memory and 50 Mbytes of disk storage space.

The NSC provide the computing environment required for the generation of the topocentric prediction data required for antenna pointing, uplink and downlink acquisition, uplink tuning control and pseudo-residual calculations. The predictions are generated using project-supplied probe ephemeris tapes (PET's) and timing and polar motion polynomials supplied on a weekly basis by the Tracking System Analytic Calibration (TSAC) group. The predictions are transmitted from the NSC via the GCF to the MDA and to the Digital Instrumentation Assembly for printout.

C. DOPPLER MEASUREMENT

The DSN Tracking System generates high precision and high stability doppler measurements. These measurements are provided to the user in the form of a non-destructive count (in cycles) of the frequency difference between a doppler reference frequency (usually the ground transmitted frequency) and the ground received (downlink) frequency.

The mechanization of the doppler generation (or extraction) process results in the following definitions:

$$\text{One-way doppler (D1)} = 48K(TSF) - AUXOSC(1 - \dot{r}_{dn}/c) + BIAS$$

$$\text{Two/three-way doppler (D2/D3)} = 48K(TSF) - 48K(TSF)(1-\dot{r}_{up}/c)(1-\dot{r}_{dn}/c) + BIAS$$

where:

K = The spacecraft coherent transponder turnaround ratio (240/221(S); 880/221(X))

TSF = The Track Synthesizer Frequency; usually the transmitted frequency or in the case of D1 simply a reference frequency approximating the spacecraft's oscillator frequency ($\sim$44MHz)

AUXOSC = The spacecraft on-board oscillator frequency

$\dot{r}$ = The spacecraft topocentric rate of change

BIAS = The doppler bias frequency ($\pm$ 1 MHz)

Hence, a spacecraft with increasing range will exhibit an increasing doppler frequency.

One-way doppler measurements are generated whenever the spacecraft is operating in a non-coherent (i.e., not transponding on the received signal) mode. Two-way doppler measurements are generated when the spacecraft is operating in a coherent mode and the ground transmit and

ground receive stations are the same. Three-way is a special case of two-way doppler with the ground receive station being different from the ground transmit station.

The process of generating a doppler measurement may be divided into two distinct phases: Doppler extraction and doppler counting.

1. Doppler Extraction

   The process of doppler extraction involves interaction between the DSS Frequency and Timing, Transmitter, Antenna Microwave, and Receiver-Exciter Subsystems. A generalized view of the process of extracting doppler is illustrated in Figure 2.

   As can be seen, the Frequency and Timing Subsystem provides precise, phase stable reference frequencies and timing pulses to the various DSS Subsystems. This frequency and timing information is primarily generated via use of hydrogen maser and cesium beam standards.

   The spacecraft downlink (appropriately multiplied and retransmitted in the two-way case) is received, amplified by the Antenna Microwave Subsystem (using low noise, 5 Kelvin amplifiers) and provided to the Receiver Assembly.

   The Exciter Assembly, using a Dana Model 7010 Synthesizer, generates the uplink frequency which is modulated with ranging and/or command data and supplied to the Transmitter Subsystem for amplification and subsequent transmission to the spacecraft. Simultaneously, the uplink frequency is provided to the Doppler Extractor Assembly for use as the doppler reference frequency.

   The phase-locked loop in normal fashion provides a measure of phase error between the local Voltage Controlled Oscillator (VCO) frequency and the received frequency. This phase error voltage is applied to the VCO to adjust its frequency to more closely match the received frequency. This VCO output frequency is essentially

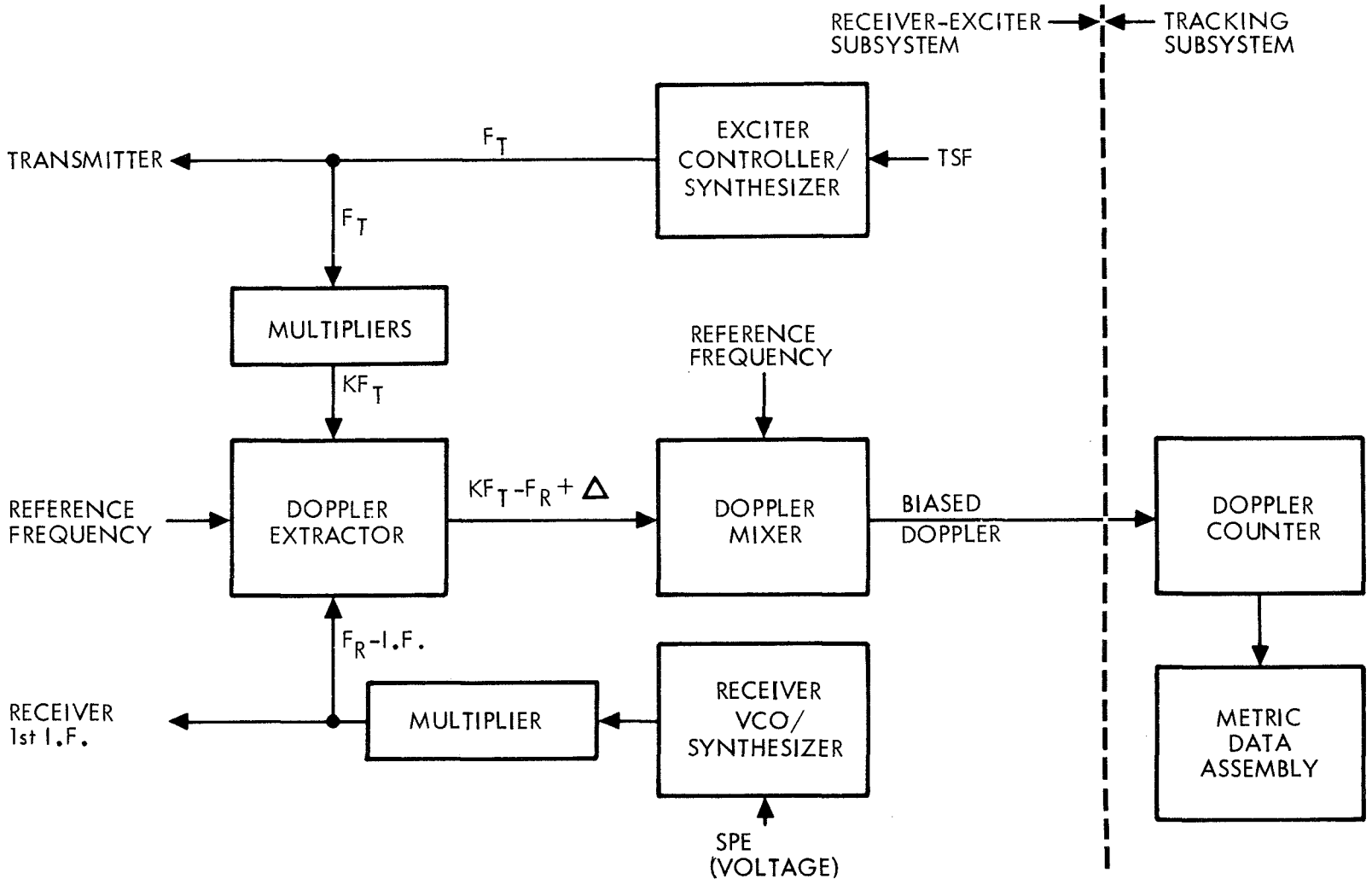

Fig. 2. Doppler Extraction

a filtered representation of the received frequency (reduced to the first IF). Since the VCO frequency is free of sidebands caused by telemetry and range modulation, it is appropriate to use this frequency for doppler extraction.

In the doppler extractor, the reference frequency provided by the Exciter Assembly is mixed with the VCO-supplied frequency and filtered to produce a biased doppler frequency. The bias (positive or negative 1 MHz) is applied to avoid problems with zero doppler conditions and band pass limitations of the hardware. Because of these hardware constraints doppler may be extracted in the following doppler shift ranges ($\Delta f/f$)=

S-Band: $\pm$ 22.2 x 10^{-4} ($\sim \pm$ 330 km/s)
X-Band: $\pm$ 6.1 x 10^{-4} ($\sim \pm$ 92 km/s)

The extracted doppler frequency is provided to the DSS Tracking Subsystem for counting.

2. Doppler Counting

The doppler counting function is performed within the special equipment subassembly of the Metric Data Assembly. The doppler count is a continuous, non-destructive count of axis crossings of the analog (sinusoidal) doppler signal. In order to ensure a precise measurement, resolver circuitry is used to determine the fractional part of a cycle that has occurred between the last axis crossing and the MDA-issued sample pulse.

This fractional cycle resolution is made by providing a measurement of the time from the sample pulse to the next axis crossing, and subtracting that time from the total cycle time. Using this method the doppler count can be resolved to an interval of approximately 1.6 nanoseconds (equivalent to 0.0016 cycles for a 1 MHz doppler frequency). The MDA samples the doppler counter and resolver at 0.1 second intervals. To provide for accurate sampling a special 10 pps timing pulse is provided by the FTS to the MDA. This pulse is stabilized to ensure jitter of no more than 2 nanoseconds.

Though continuously sampling at 0.1 s intervals, the MDA only transmits the count coinciding with the user-selected sample interval, which ranges from 0.1 s to 600 s.

D. DOPPLER MEASUREMENT PERFORMANCE

As mentioned in the introduction, the DSN Tracking System undergoes a continuous evolutionary process in order to meet the ever more demanding requirements imposed by the various spaceflight projects. One measure of the tracking system performance is the system fractional frequency stability ($\Delta f/f$). The improvements in this parameter are illustrated in Figure 3. As can be seen, the stability of the system (hence, the accuracy of the measurements) has improved by approximately five orders of magnitude from 1960 to the present. This improvement has been the result of higher link frequencies (L-band to S-band to X-band) and a multitude of equipment improvements (e.g., hydrogen maser timing standards, improved doppler extractors, doppler resolvers, etc.)

Another measure of tracking system performance is the uncertainty or noise introduced into the measurement by the various assemblies and subsystems involved in the process of generating the doppler measurements. This parameter has also been affected by the various improvements to the Tracking System.

The doppler phase noise may be characterized by the equation:

$$\sigma_{dop} = \left[\sigma_R^2 + \sigma_T^2 + \sigma_Q^2 + \sigma_E^2 + \sigma_D^2 + ((\Delta f/f)(f_r)(t_s \text{ or } RTLT))^2\right]^{1/2}$$

where:

σ_R^2 = the receiver contribution including thermal noise, internal noise, synthesizer noise, etc. This value is typically $\sigma \leq 12^o$.

σ_T^2 = the noise due to timing jitter. As previously mentioned, special timing pulses are provided which keep this value to an absolute minimum. Typically this value is $\sigma \leq 0.2^o$ (1 MHz).

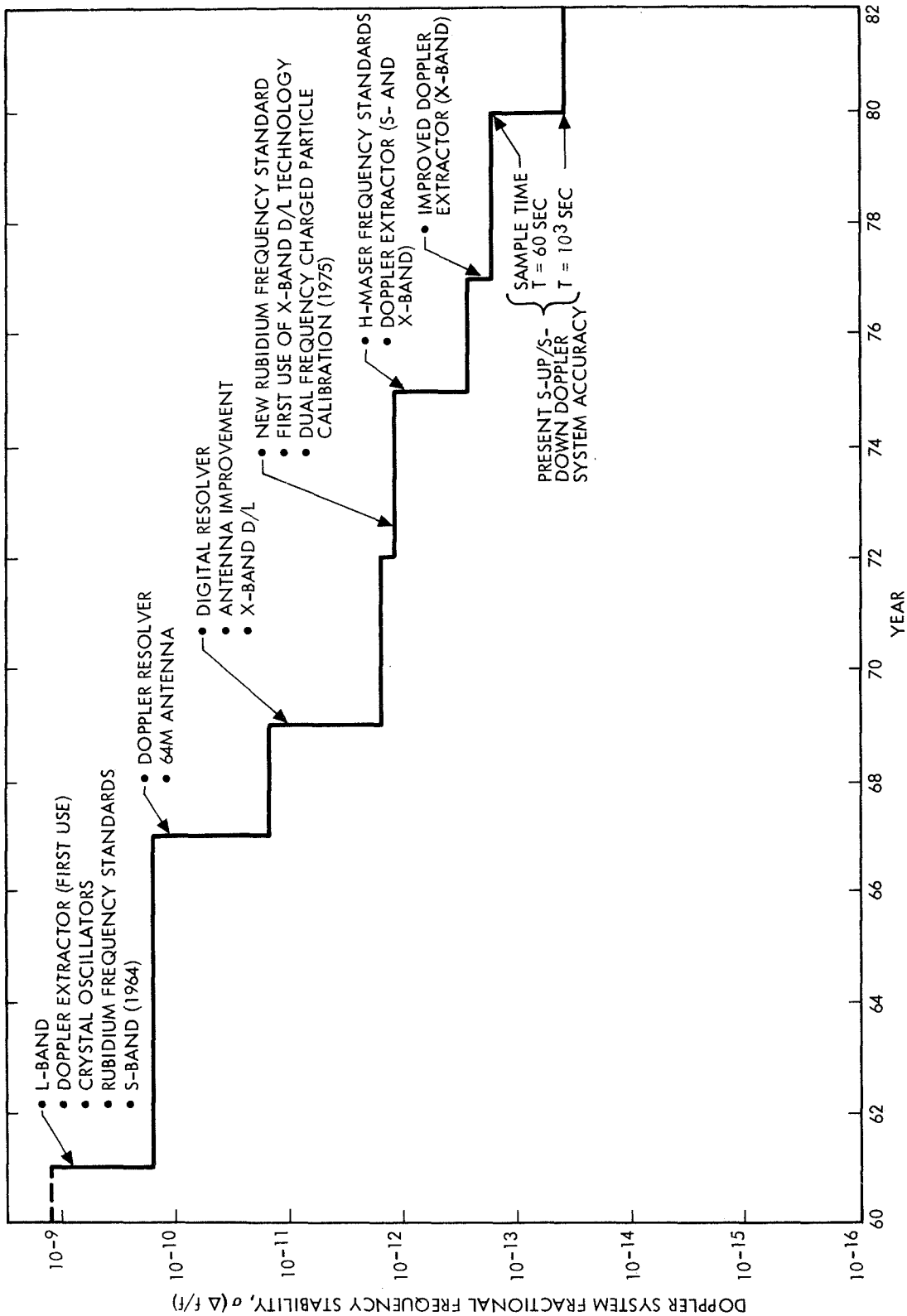

Fig. 3. Tracking System Accuracy Improvement

σ_Q^2 = the quantization error of the doppler counter. Use of the resolver circuitry reduces this figure to $\sigma \leq 1^o$ (1 MHz)

σ_E^2 = the phase noise induced by the doppler extractor. This parameter varies according to signal level with $\sigma \leq 4^o$ for signal margins of 40 dB.

σ_D^2 = phase noise induced by changes in the path delay of the ground equipment. This parameter typically has effects only over long count intervals.

$((\Delta f/f)(f_r)(t_s \text{ or RTLT}))^2$ = the frequency standard instability measured over either the sample time (t_s) or the RTLT, whichever is shorter. With the use of highly stable hydrogen maser standards, the $\Delta f/f$ parameter approaches 8×10^{-13} over 10000 seconds.

The sum of these parameters may be seen in Figure 4, the X-band doppler phase uncertainty versus count time, and Figure 5, the S-band doppler phase uncertainty versus count time. Periodic system performance tests are run to ensure that the doppler system performance corresponds to values depicted in these curves.

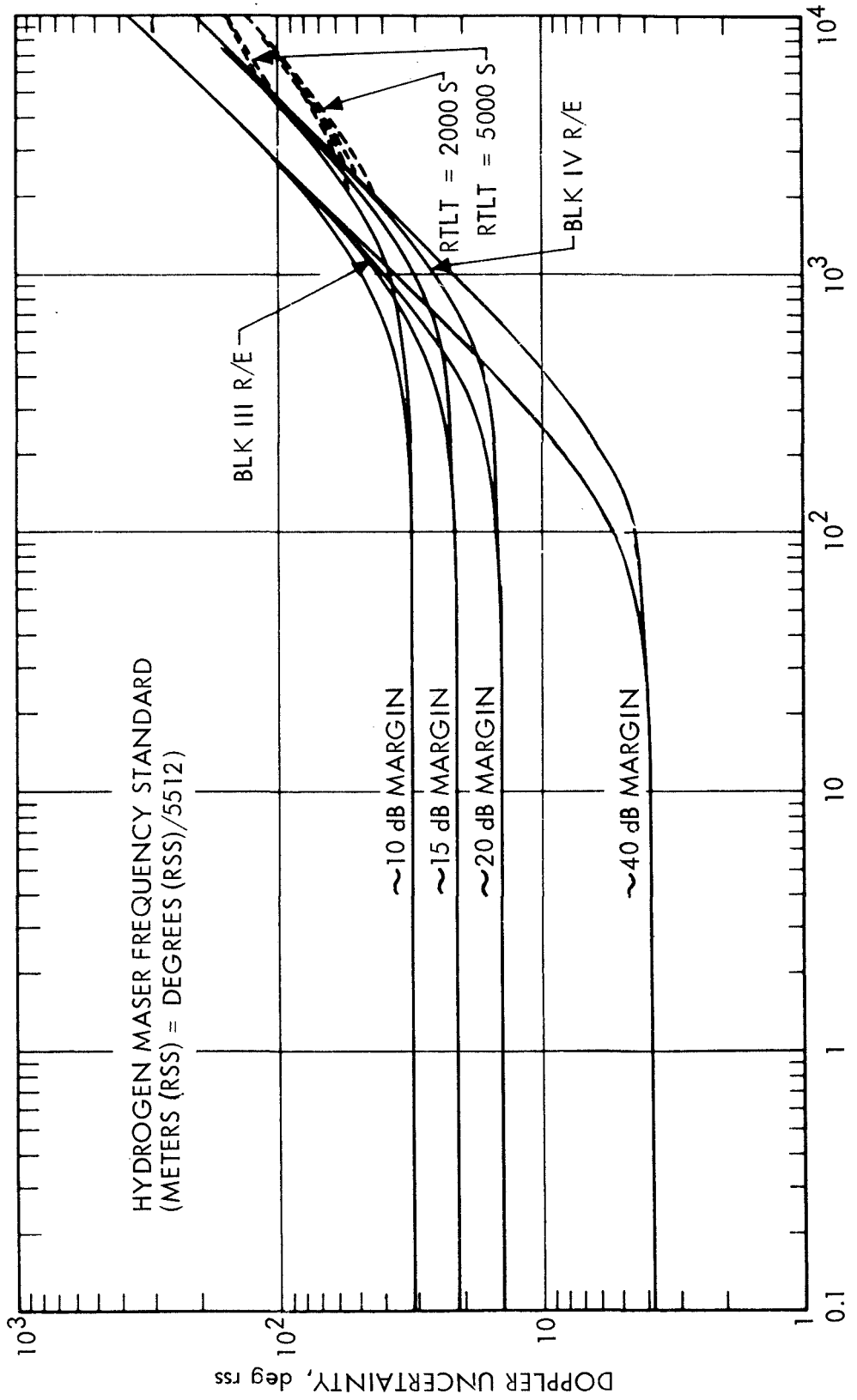

Fig. 4. X-Band Doppler Phase Uncertainty Versus Count Time

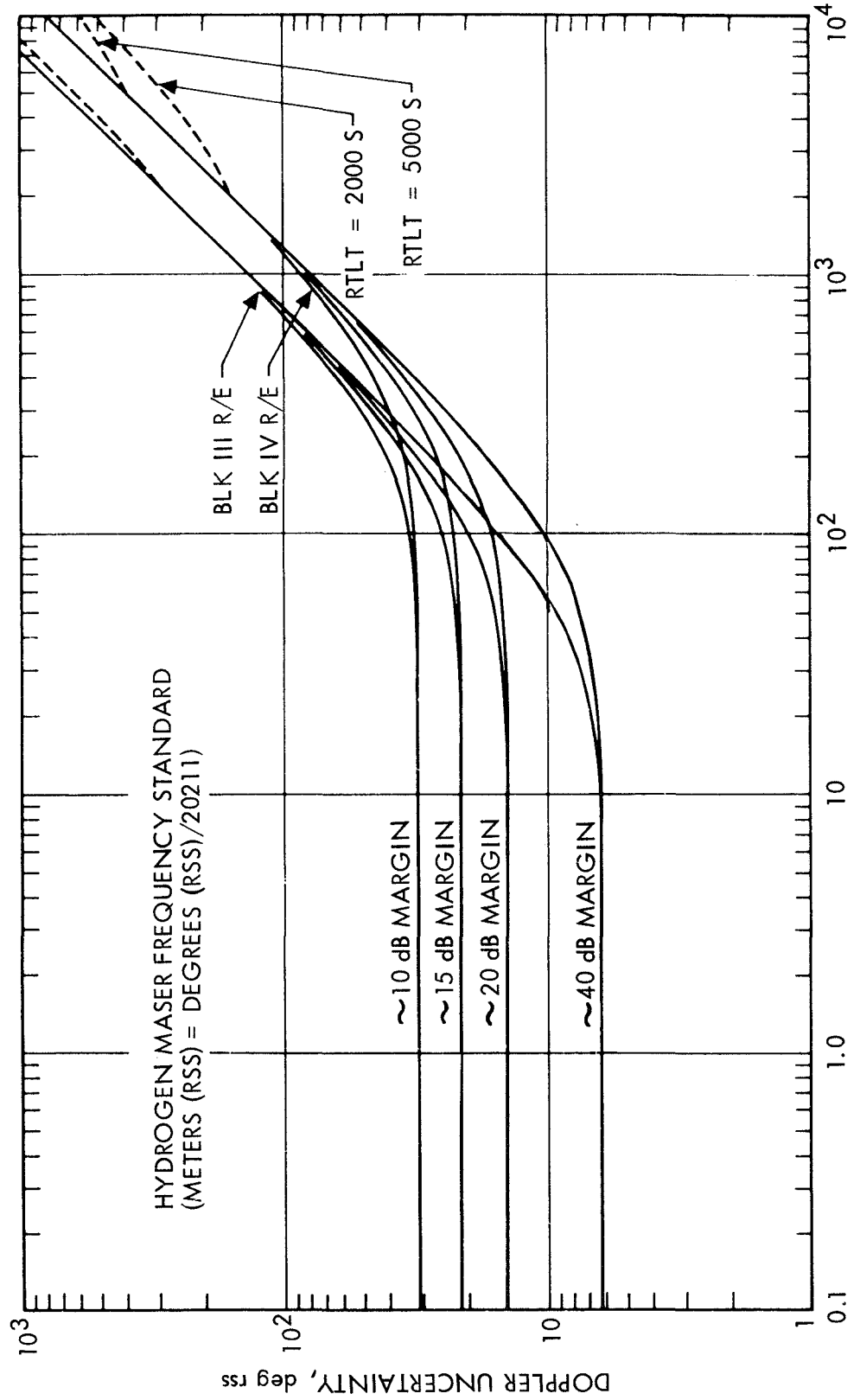

Fig. 5. S-Band Doppler Phase Uncertainty versus Count Time

E. DSN RANGE MEASUREMENT

The Network uses a binary coded sequential acquisition ranging technique to provide an indirect measurement of the (backward-looking) round-trip-light-time (RTLT) between the station and the spacecraft. This measurement, termed a range measurement, is generated by the Planetary Ranging Assembly of the DSS Tracking Subsystem.

The basis for the range measurement is the fact that a repeating range code modulated onto the uplink carrier and transmitted to the spacecraft, then retransmitted to the ground station, will be out of phase with the originally transmitted range code. Given that the period of the range code is greater than the RTLT to the spacecraft, the phase difference translates directly into a measure of the station-to-spacecraft range. Because of the great distances involved in planetary exploration, it is not practical to transmit range codes including frequencies with these long periods (resolution of the range to a spacecraft at Jupiter would require transmission of a code with frequency $\sim$ 0.0002 Hz). An a priori estimate of the range is made, therefore, and the actual range measurement simply resolves the ambiguity of the estimate.

The DSN range point is then the measurement of the position of the spacecraft within a modulus determined by the period of the lowest frequency component of the range code. In equation form:

$$\text{RANGE DSN} = 48\,F_T(\text{RTLT}) - M(2^{N+10}) + \text{BIAS}_{DSS} + 48F_T(\text{BIAS}_{S/C} - Z) \quad (1)$$

where

$48F_T$	=	Range Unit Conversion Factor
F_T	=	(Ground) Transmitted Frequency (~ 22MHz)
1 RU	=	$1/(48 \times F_T)$ = 0.95 Nanoseconds (2 way)
RTLT	=	Round Trip Light Time to/from the Spacecraft
M	=	A priori estimate of the number of moduloes in the distance (round trip) to the spacecraft
2^{N+10}	=	Number of range units per modulo
N	=	Number of the lowest frequency component
BIAS_{DSS}	=	Measured Station Delay (RU)
$\text{BIAS}_{S/C}$	=	Measured Spacecraft Delay (nanoseconds)
Z	=	Measured Delay to DSS Reference Location (nanoseconds)

The range code as transmitted by the DSS consists of a sequentially transmitted series of frequencies. Each successive frequency is related to the previous frequency in a binary power (2^N) sense and is phase coherent with it. The periods of the transmitted frequencies are directly tied to the transmitter frequency. Hence, a change in transmitter frequency results in a change, in direct proportion, of the code frequency. The range measurement is likewise related to the transmitted frequency by utilizing the range unit as the fundamental unit of measurement; one range unit is $1/(48 \times F_t)$ or two wavelengths of the transmitted frequency.

The typical sequence of frequencies consists of a "clock" frequency followed by a series of "code" frequencies. The "clock" is the highest frequency component and is used to make the initial phase determination and provide the precision of the range measurement. The "clock" frequencies available are: ~1 MHz (zeroth component), ~500 KHz (first component), ~125 KHz, and ~31 KHz. The 1 MHz component provides a resolution of ~1 nanosecond. This component is transmitted for a period of time determined by the available ranging signal power and the user-required measurement noise level.

The "code" components consist of the frequencies following the highest frequency component. These frequencies span from ~500 KHz to ~1 Hz depending on which "clock" is in use. The lowest frequency component is used to resolve the ambiguity (or uncertainty) in the a priori range estimate with the largest resolvable ambiguity being ~150000 km (clock period ~ 1 s) and the smallest resolvable ambiguity being ~290 m (clock period ~ 2 μs). The code components are each transmitted for the same length of time determined by the available ranging signal power and the acceptable probability (as determined by the data user) of error in determining the phase of the code component.

As the range code progresses to lower frequencies the possibility of causing interference with command and telemetry subcarriers and of being tracked out by either the spacecraft or DSS receiver's phase-locked loop increases. To avoid this problem, the code components are chopped with the highest frequency ("clock") component. This effectively causes the

signal power of the code component to be concentrated near the sum of the "clock" and "code" frequencies.

Table I provides equations which describe measurement capabilities of the Network ranging equipment.

The generation of a range measurement begins by selecting the appropriate highest (resolution) frequency and lowest (ambiguity) frequency components and the integration times required to meet the noise and power availability constraints. The individual frequency components are successively phase modulated onto the uplink carrier and transmitted to the spacecraft. At the spacecraft, the components are demodulated, then remodulated onto the coherent downlink carrier. At the ground station, the downlink carrier is focused, amplified and then tracked by the receiver. The receiver supplies an intermediate frequency modulated by the range components to the Ranging Demodulator Assembly (RDA). At this point the originally transmitted range component frequencies have been modified in frequency by doppler, in phase by the range and in both frequency and phase by the transmission media.

The shift in frequency due to the doppler effect is accounted for by doppler rate aiding the reference (transmitted) range code. That is, the extracted doppler is applied to the reference code, resulting in a reference code which is frequency coherent with the received code. The time at which this coherency is established is termed t_o and is also the time for which the computed range point is valid.

The shift in phase due to range is precisely the parameter desired to be determined. To measure the phase shift, the highest frequency components of the received code and reference code are compared and a correlation voltage dependent on the phase difference is generated. The voltage is periodically sampled and summed over the integration time. Simultaneously, a comparison is made with the reference code shifted 90^o to provide a quadrature channel. Figure 6 shows the correlation voltage versus phase for the in-phase and quadrature reference codes. The phase offset is quickly calculated by the Planetary Ranging Assembly from the correlation voltages.

Table I.

DSN Range Measurement Equations of Interest

Period of N^{th} component	:	$(64X2^N)/3F_T$
ns/RU (2 way)	:	$1/(48\ F_T)$
m/RU (2 way)	:	$C/(48\ F_T)$
Approximate Ambiguity Resolving Power (meters)	:	$(C/2)(64X2^N)/3F_T$
Precision of Range Measurement (meters)	:	$(C)(64)/(3F_T)(1024)$ Clock 0 $(C)(64X2^N)/(3F_T)(2048)$ Clocks 1, 3, 5
Length of Modulo (2 way)	:	2^{N+10} (Range Units)
High Frequency Component Integration Time (T1)	:	$(P/2)^2/(32(\sigma/C)^2(P_R/N_0))$
Other Components Integration Time (T2)	:	$(ST_2/N_0)/(P_R/N_0)$
Total Acquisition Time	:	T1 + (Number of Components -1)T2

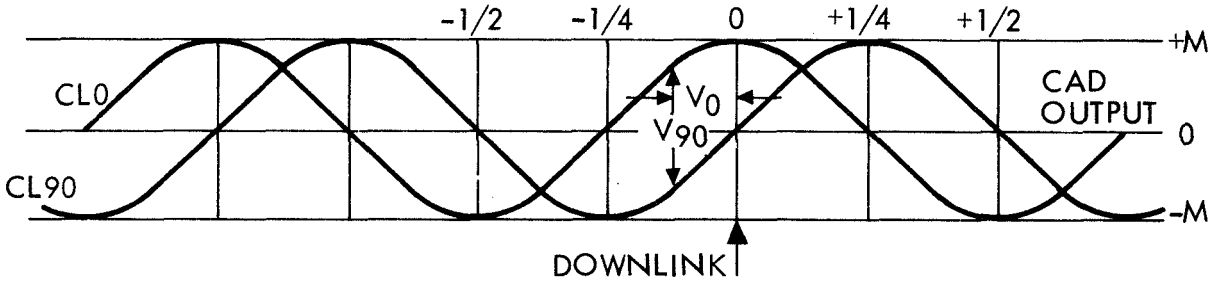

$$\sqrt{(V_0)^2 + (V_{90})^2} = M \text{ (A CONSTANT)}$$

V_0 = CLOCK 0°

V_{90} = CLOCK 90°

SINEWAVE CLOCK

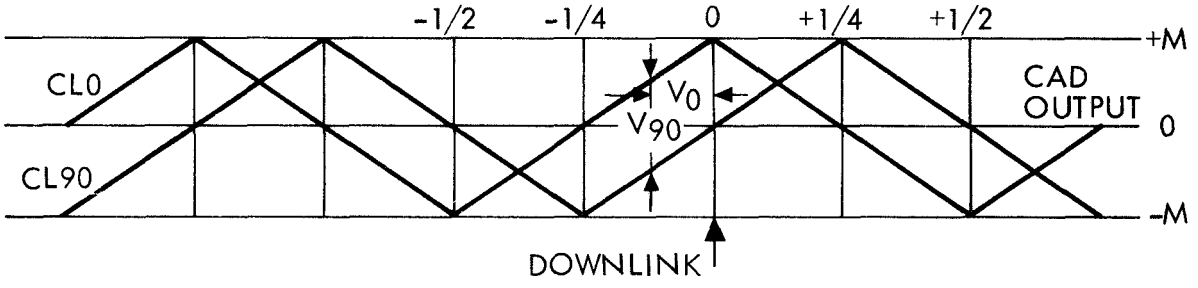

$$|V_0| + |V_{90}| = M \text{ (A CONSTANT)}$$

SQUAREWAVE CLOCK

Fig. 6. Correlation Voltage versus Phase

Because of the ambiguities of the high frequency component, the computed phase delay (τ) is satisfied by any of the points (A through D) in Figure 7. Assuming that point A satisfies the phase offset, the value of τ is saved. The ambiguity is then resolved by the low frequency component of the range code.

Since the remaining frequencies are generated using a binary adder they are phase coherent. Thus, it is necessary only to determine if each successive component is in phase or 180^{0} out of phase with the previous component.

In the example, it can be seen from the correlation function that at point A, the second component is at a negative peak and thus out of phase. The reference code is then shifted by half the period of the component (to point B) to bring it into phase. If the component was already in phase no shifting would be required. At point B, the C3 correlation is determined to be out of phase with C2. Thus the reference code is shifted by half the period of C3 to bring it to point D. The total phase shift then is τ_R, the phase displacement between point A and point D. Converted to range units, this displacement is the indirect measure of the range.

The shift in frequency and phase due to media effects may be partially determined by reacquiring the highest frequency component. This remeasurement of the phase delay provides a parameter termed Differenced Range Versus Integrated Doppler (DRVID).

1. Ranging Calibration

   From equation (1), it can be seen that the DSN range point measures the total range including the station and spacecraft components. To arrive at the range referenced to the station location (usually the intersection of the antenna axes) these components must be removed from the measurement prior to using the data.

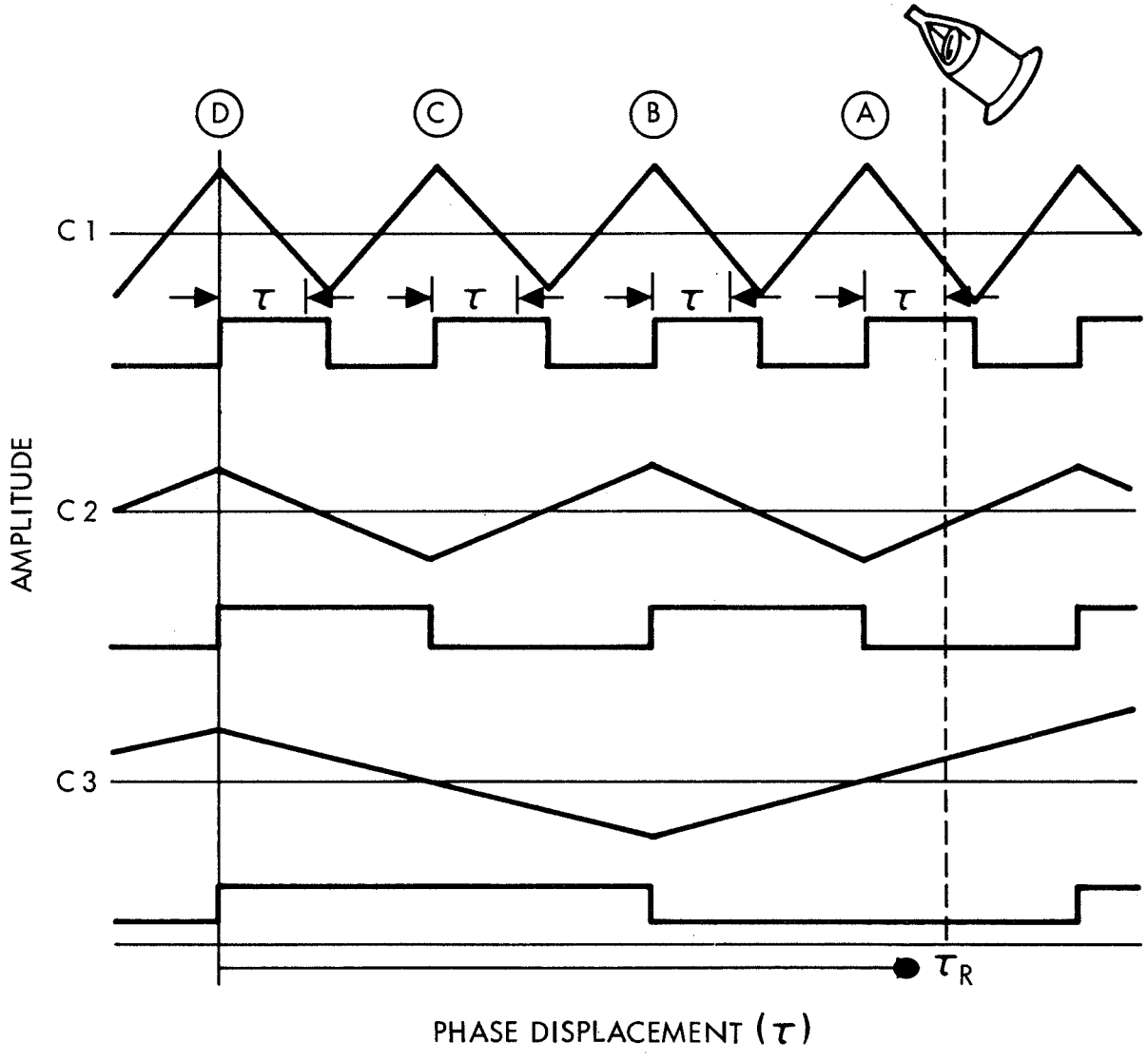

Fig. 7. Computed Phase Delay

The spacecraft delay is typically measured during prelaunch compatibility testing.

The station delay is regularly measured by DSN personnel. This delay consists of two components: the DSS delay and the Z correction. The DSS delay is configuration dependent and is measured prior to each spacecraft track. This delay is measured by using the actual ranging equipment and transmitting through a test translator to allow the signal to traverse the same path (as much as possible) followed during actual spacecraft ranging. As can be seen in Figure 8, this delay includes the component delays of all the appropriate station hardware except the microwave waveguides, airpath, and miscellaneous components forward of the calibration signal injection point.

The Z-correction (illustrated in Figure 9) includes the delays caused by the waveguides, airpath and other components forward of the test signal injection point, as well as that of the test translator (used in the measurement of the DSS delay) and the difference betweeen the antenna aperture plane and the reference location. The Z-correction is typically determined by physically measuring or precalibrating the hardware components prior to installation.

2. Ranging Error Allocation

Typically range data accuracy requirements are quite stringent. The Voyager project, for example, required two-station accuracy of $4.5\ \sqrt{2}$ meters. In order to meet these requirements, the tracking system is regularly calibrated and limits on allowable errors are specified for all components of the ranging path. The error allocations for the major subsystems and assemblies involved in ranging are shown in Table II.

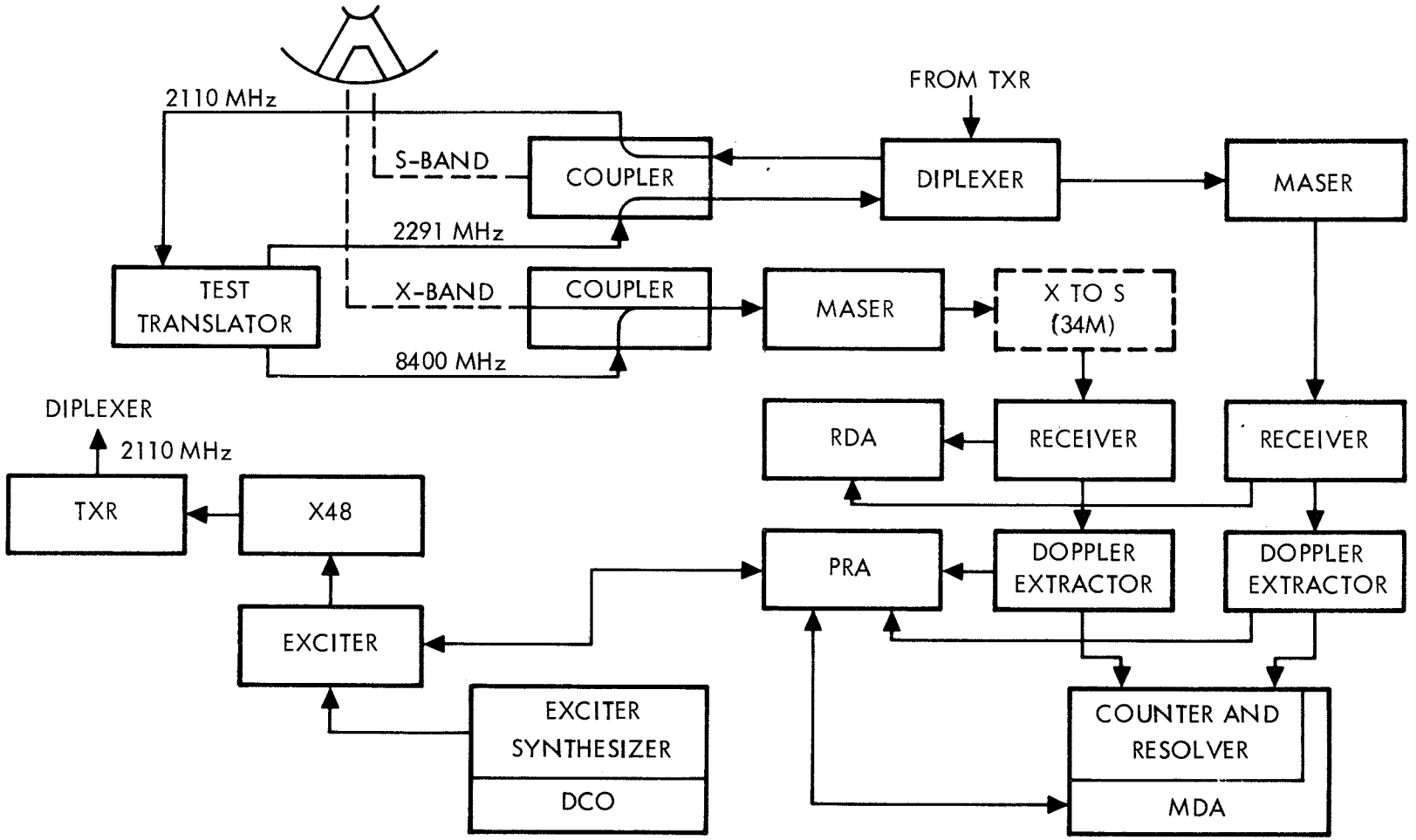

Fig. 8. DSS Range Delay

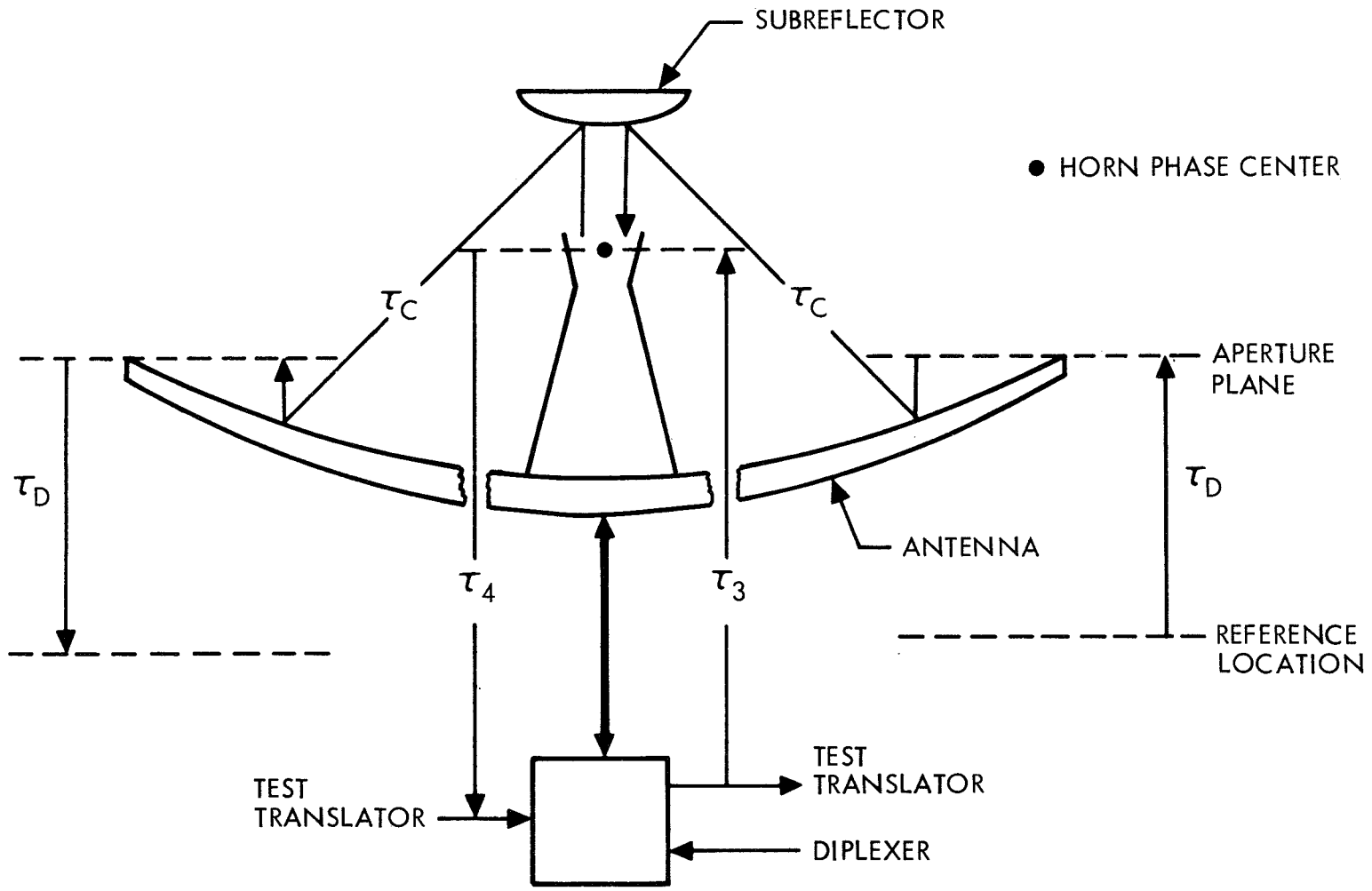

$$Z_{CORRECTION} = \tau_{XLATOR} - (\tau_3 + \tau_4 + (\tau_C - \tau_D)_{UP} + (\tau_C - \tau_D))$$

Fig. 9. Z Correction

Table II. DSS Ranging Error Allocation (1σ , meters)

Subsystem/Assembly	34m DSS	64m DSS
Frequency and Timing Subsystem	2.0	0.3
Receiver-Exciter Subsystem	1.1	0.5
Transmitter Subsystem	1.1	0.5
Microwave Subsystem	1.1	0.6
DSS Tracking Subsystem	0.3	0.3
Ranging Calibrations	1.0	1.0
Cables	0.4	0.1
TOTAL (RSS)	3.0	1.4

III. THE DSN VLBI SYSTEM

A. INTRODUCTION

In response to navigational requirements levied by the Voyager Flight Project, the DSN in early 1978 brought into existence the DSN VLBI System. Specific Voyager Project requirements included:

1. Interstation time synchronization: 10 microseconds
2. Master clock stability: 3×10^{-13} over 1000 seconds
3. Universal Time One: 1.25 milliseconds
4. Polar Motion: 50 centimeters
5. Hydrogen Maser Monitor performance: 10 nanoseconds
6. Δ DOR: 30 centimeters (corresponding to time delay)

The initial configuration of the DSN VLBI System, referred to as "Mark I-79," provided the capability to meet all requirements except for Δ DOR. New implementation in 1981 resulted in a new configuration, "Mark II-81," which provided the Δ DOR capability. The equipment elements necessary to generate VLBI data are located at the three 64-m antennas (Goldstone, California; Madrid, Spain; and Canberra, Australia). The data are transferred via the Ground Communications Facility (GCF) to the JPL Network Operations Control Center, where the correlation facilities are located. Figure 10 is a functional block diagram of the VLBI system.

The equipment at these locations consists of elements from the existing Advanced Equipment Subsystem (AES) and implemented assemblies of the DSS VLBI Subsystem. The AES contains assemblies which were initially installed for use by the advanced VLBI system development group. The VLBI Subsystem provides additional digital processing assemblies and means of data transmission via the Wideband Data Lines (WBDL) of the GCF to permit immediate data correlation at the VLBI correlator.

The VLBI System is undergoing continued evolution and implementation to augment this initial configuration and will provide an operational system with more accurate and flexible capabilities.

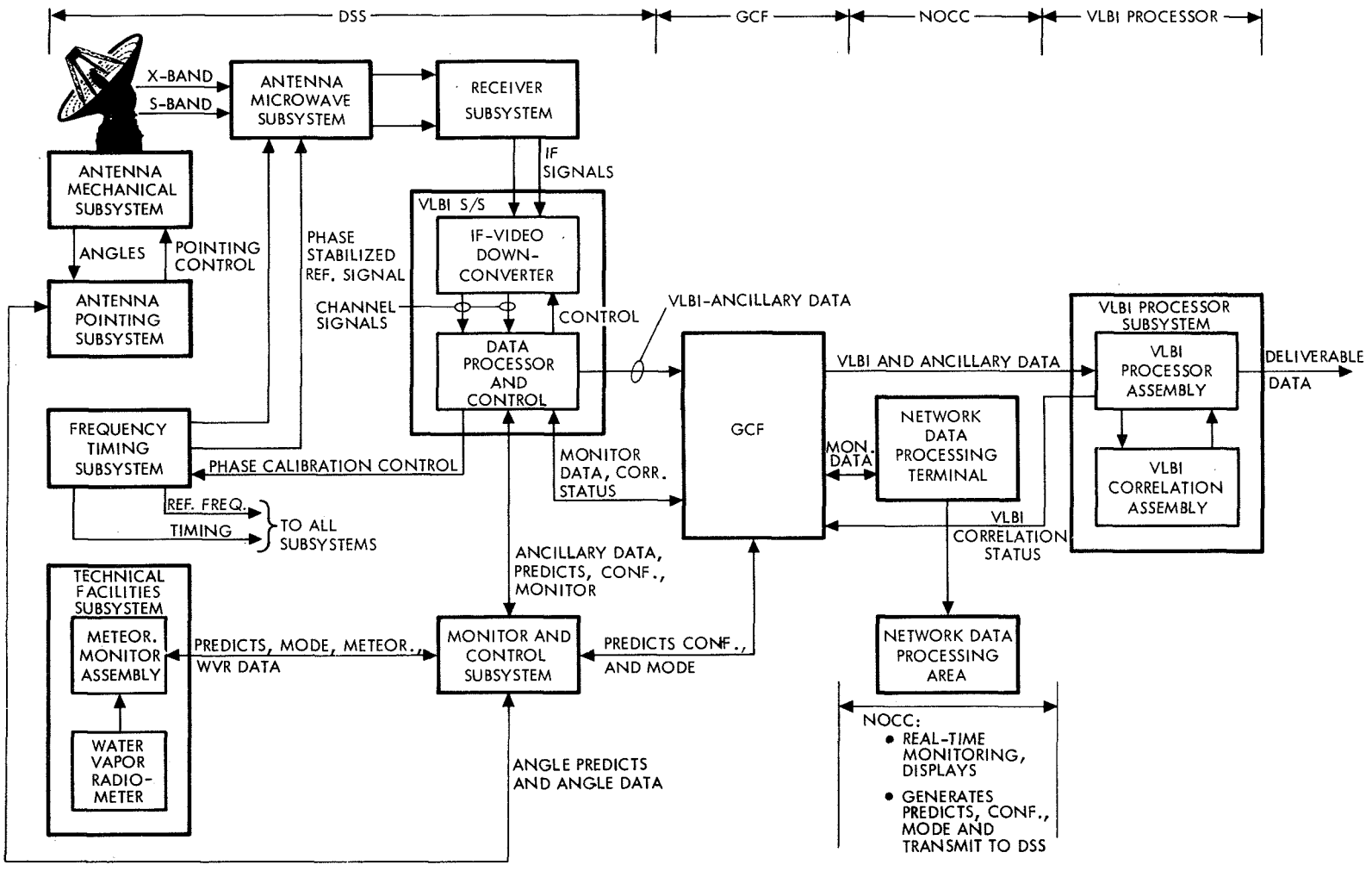

Fig. 10. VLBI System Functional Block Diagram

B. THE VLBI OBSERVABLE

The process of Very Long Baseline Interferometry is described briefly as follows (Thomas, 1972):

The radio signal produced by a distant source is received and recorded simultaneously at two radio antennas. Because of a difference in raypaths, the signal will arrive at one antenna some time interval after it reaches the other. By cross correlating the two recorded signals, this time delay and/or its time derivative may be determined. In addition, correlated amplitude measurements can yield information concerning source strength and structure. If the radio signal is generated by an extragalactic object, the radio source may be regarded as a fixed object because of its great distance. In this case, the time variation of the delay is due to the Earth's motion and depends on the source location and the baseline vector between the two antennas. Measurements of the time delay and/or its derivative for many sources can be used in a least-squares determination of source locations, the baseline vector, and Earth orientation parameters, such as UT1 and polar motion.

Consider two antennas separated by a distance (baseline) B receiving a signal from a distant extraterrestrial source. The geometry is shown in Figure 11. If the source is assumed to be monochromatic and noise (receiver and background) is neglected, the received signals at the two antennas can be represented as (Molinder, 1978)*:

$$V_1(t) = A_1 \cos 2\pi f_s t$$

and

$$V_2(t) = A_2 \cos 2\pi f_s (t - \tau_g)$$

with

$$\tau_g = (B \cos \Psi)/c$$

*Assumes zero instrumental delay

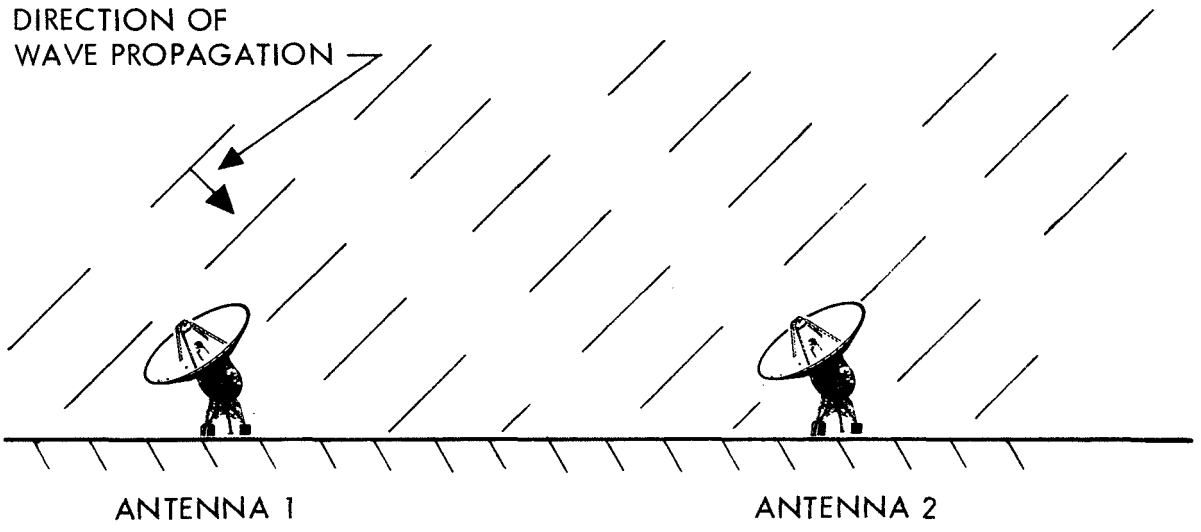

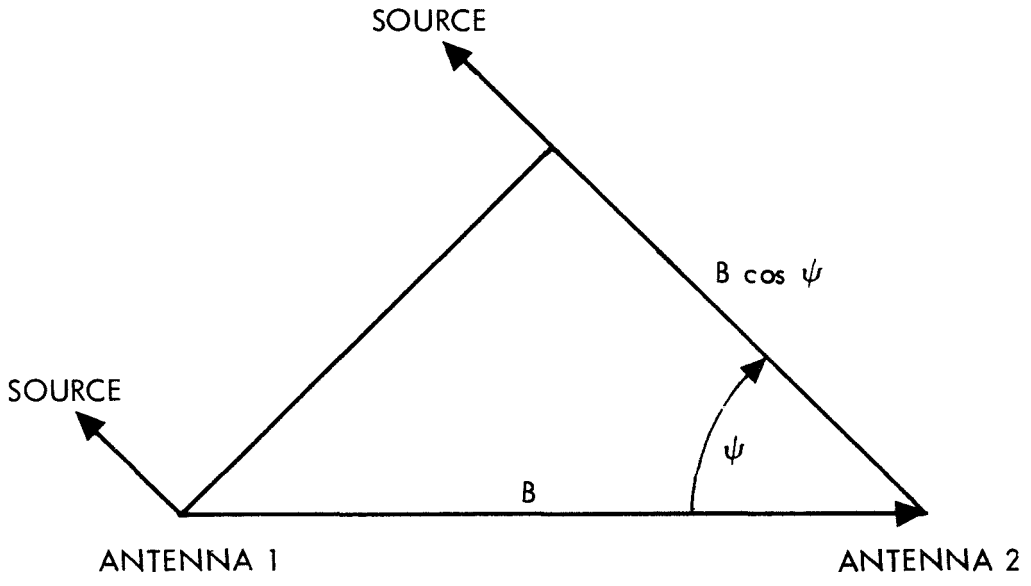

Fig. 11. VLBI Geometry

where

A_1, A_2 = strength of the received signals at antennas 1 and 2, respectively

τ_g = time delay (typically a slowly varying function of time due to the earth's rotation) in the reception of a given wavefront at antenna 2 relative to antenna 1

c = velocity of light

ψ = angle between baseline and source

B = baseline length

V_1, V_2 = time-varying received signals from antennas 1 and 2

f_s = received frequency

t = time

The signals V_1 and V_2 are correlated to produce an initial time delay estimate and fringe phases in each channel. The channel phases are then combined in a process called bandwidth synthesis to obtain a precise delay τ_g. The resulting uncertainty in τ_g is given by:

$$\sigma_{\tau_g}(\text{cm}) = (K_2/B_s J d_1 d_2) \sqrt{T_{s1} T_{s2}/\varepsilon_1 \varepsilon_2 S_r T} \quad \text{cm}$$

where

B_s = spanned bandwidth in MHz

J = correlated flux of radio source in Janskys

ε_i = antenna efficiency $i = 1, 2$

d_i = antenna diameter in meters

K_2 = 3.72×10^4

T_{s1}, T_{s2} = total system noise temperature (K) at antennas 1 and 2 respectively

S_r = mean sampling rate in Mbits/s for each channel

T = total integration time in s

As an example, using the following values for a typical Mark II observation,

$K_2 = 3.72 \times 10^4$
$J = 1$ Jansky
$T_{s1} = T_{s2} = 30$ K
$S_r = 4$ Mbps
$B_s = 40$ MHz
$d_1 = d_2 = 64$ m
$_1 = _2 = 0.55$
$T = 150$ sec (2-1/2 min)

yields

$$\sigma_{\tau_g}(\text{cm}) = (3.72 \times 10^4/(40)(1)(64)(64)) \sqrt{(30)(30)/(0.55)(0.55)(4)(150)}$$
$$= 0.5 \text{ cm}$$

Again it is important to note that the above equation gives the standard deviation in the measurement of the delay τ_g due to thermal noise only. Other error sources such as instrumental effects, propagation (ionosphere), modeling, etc., must also be considered. The real importance of the equation is to show the manner in which various parameters affect VLBI accuracy.

To further consider the effect of other error sources on baseline measurement, there is the following approximate relationship:

$$\sigma \simeq \sigma_x A \sqrt{N_p/N_{obs}}$$

where

N_p = number of parameters solved for in the multiparameter fit
N_{obs} = number of observations
A = constant ranging from 2 to 4 depending on a covariance analysis based on source locations, etc.

and

$$\sigma_x^2 = \sigma_{\tau_g}^2 + \sigma_o^2$$

where

σ_{τ_g} = that given previously

σ_o = standard deviation of other uncertainties such as ionospheric effects, tropospheric effects, uncertainties in source positions (if taken as given), frequency standard deviations from linear performance in time, etc.

For example, consider solving for three earth parameters and four clock parameters using 28 observations, with σ_{τ_g} = 0.5 cm (see previous calculation) and A = 4. Assume for simplicity that σ_o = 0; then

$$\sigma = (0.5)(4) \quad \sqrt{7/28} = 1.0 \text{ cm}$$

Since the number of bits required (N_T) is

$$N_T = N_{obs} S_r T$$

then the total number of bits required in this case is given by

$$N_T = N_{obs} S_r T = 28 \times 6 \times 10^8 = 1.68 \times 10^{10} \text{ bits}$$

1. VLBI Application

When used for conventional (non-differential) VLBI, the DSN VLBI System observes Extra-Galactic Radio Source (EGRS) signals using two or more antennas. From the measurements of the difference in the time of arrival of the EGRS signal between the antennas, the position of the radio sources can be determined as can several other parameters. These other parameters include Universal Time One (UT1), Earth polar motion, the relative position of the observing stations, time offset, and the rate of change of the station clocks (clock synchronization and frequency stability of the station's frequency standards).

2. VLBI Application

When used for differential VLBI (Δ VLBI), the DSN VLBI System alternates observations of an EGRS signal and the signal from a deep space spacecraft transmitter, again using two or more antennas. There are two types of Δ VLBI: single-channel and multiple-channel.

In single-channel Δ VLBI, the phase delay (phase shift) of the signal is the desired data obtained within a single narrow-band segment of the radio frequency (RF) spectrum. The phase rate provides a direct measurement of the delay rate and is analogous to a differenced doppler measurement between stations.

In multiple-channel or wide bandwidth Δ VLBI, the phase delay is obtained from a number of narrowband channels. The narrowband channels are separated within the RF spectrum across a wide span bandwidth. The phase delay measurements from the individual channels are combined to determine the group delay over the spanned (separated) bandwidth. This method of obtaining the wide bandwidth group delay from individual narrow bandwidth channels is termed Bandwidth Synthesis (BWS). The group delays are then used to determine the differential geometric time delay (group delay) between the alternate source signals. This is analogous to a doubly differential range measurement between sources and stations and is known as delta differential one-way range or Δ DOR.

The separate segment bands for Δ DOR application are centered at the subcarrier frequencies of the spacecraft signal. These line spectra sidebands are created by modulating the carrier with baseband signals of 0.765, 3.825, and 19.125 MHz (these signals are the planned frequencies for Galileo).

The VLBI System downconverts the RF channels (sideband line spectra) individually to a data channel bandwidth (BW) of video-band frequencies (a typical video BW is 40 kHz to 250 kHz). This is the response of the Narrow Channel Bandwidth (NCB). During the observation of the EGRS continuous spectrum signal, the same frequencies as acquired from the spacecraft are downconverted, and the EGRS signal group delay is obtained

by the same BWS process. The spacecraft and EGRS delays are then differenced to produce a quantity which is a function of the spacecraft position with respect to the EGRS. This differential observation tends to cancel any errors produced by the intervening propagation media and the observing stations' electronic equipment and location.

C. FUNCTIONAL DESCRIPTION OF VLBI SYSTEM

Although the DSS portion of the VLBI system is still undergoing various implementation phases, this description applies to the system's functional characteristics. The DSSs individually receive the RF signal and down-convert segment bandwidths of the RF spectrum to video-band frequencies, which are then digitized and formatted by digital equipment. The digital data are then transmitted via the GCF to the NOCC and to the VLBI processing area for signal processing with data from other observing stations.

The DSS Antenna Subsystem is pointed to the appropriate signal source at the proper time by the Antenna Pointing Subsystem, which obtains pointing information (predicts) from the NOCC Support Subsystem (NSS) via the GCF.

The Antenna Microwave Subsystem (UWV) receives the signal flux gathered by the antenna. After amplification by the Traveling Wave Maser (TWM) the signal is sent to the Receiver-Exciter Subsystem.

The VLBI System is capable of receiving span bandwidths of 40 MHz at S-band and 100 MHz at X-band. The actual frequency bands are 2265 to 2305 MHz for S-band and 8400 to 8500 MHz for X-band. Signal polarization is right hand circular.

The Frequency and Timing Subsystem (FTS) provides the station local clock, using a hydrogen maser as the primary standard. Reference frequencies and timing signals are derived from the clock for distribution to other subsystems. Similarly, a reference signal from the coherent reference generator (CRG), which distributes the reference signals, drives the Phase Calibration Generators (PCG) located within the Antenna Microwave Subsystem via a coaxial-cable, phase-stabilization assembly which

effectively translates the station's clock frequency stability to the comb generators. The comb generator within the PCG provides comblike, phase-stable, line spectra at S- and X-band microwave frequencies, which are injected into the input circuitry of the TWMs.

These phase-stable reference signals are amplified by the TWM and are downconverted simultaneously with the received signals. These reference signals are used to calibrate phase variations (which occur within the TWM, receiver, downconverter, and digital subsystems) during the cross-correlation and data processing procedure. The comb signals encounter the received signal for the first time at this injection point, and since the effective signal propagation delay from this point to the antenna location reference point (intersection of axes for the 64 m antenna) is accurately measured at each station, the calibration can be translated to this antenna point. Thus, the antenna location point serves as the reference point to which the cross-correlation and post-correlation estimation calculations relate to other Deep Space Stations the resultant earth parameters, such as antenna location, UT1, and polar motion. Similarly this reference can be related to the Epoch reference point at the FTS CRG output located within the control room. The cable stabilizer effectively translates this point with a known time delay for interstation clock synchronization purposes. The clock Epoch reference point in turn will function as the reference for all subsystems and assemblies within the respective stations.

The receiver IF signal is input to the DSS VLBI Subsystem (DVS) IF-to-video downconverter assembly. The video band spectrum of the various reference channels is then digitized and passed through a low-pass filter (LPF) which completes the BWS process and produces the VLBI data.

The VLBI data are further formatted for transmission to NOCC. The DVS provides a real-time record of the data as well as control to the other assemblies of the VLBI System to ensure proper configuration during the operational sequence. It also receives ancillary data from other DSS Subsystems; these data are forwarded to NOCC for performance monitoring and to the processing area for use in data processing.

Ancillary data, which are sampled and recorded with the VLBI data, consist of the following:

1. VLBI predicts
2. Subsystem configuration, status, and data mode
3. Angles and angle residuals
4. Recorder status
5. Ground weather data
6. Water vapor radiometer data
7. Ionosphere data

Configuration, status performance, and data mode are transferred from the relevant subsystem to the DVS for inclusion with the ancillary data. Monitor data are also be routed to the DSS Monitor and Control Subsystem (DMC) for DSS operations display together with other ancillary data.

Monitor data from DVS are transmitted via High Speed Data Line (HSDL) to the NOCC Radio Science Subsystem (NRS) Real-Time Monitor Assembly (RTM) for display to and evaluation by the Network Operations Control and the Network Analysis Teams. These monitor data are the VLBI-related subsystem parameters and all of, or a subset of, the ancillary data.

Station weather and WVR data, which are obtained by the Meteorological Monitor Assembly (MMA) of the Technical Facilities Subsystem (FAC), are sent to the DSS Monitor and Control Subsystem (DMC). This information, together with the antenna angles sent from the Antenna Mechanical Subsystem (ANT), is forwarded to the VLBI Subsystem and is included with the VLBI data which are provided to the station Wideband Data Assembly of the GCF.

The antenna pointing predicts are generated by the prediction software within the NOCC Support Subsystem (NSS), using the Radio Source Catalog, and are received from the NSS via the GCF. These predicts are then used to direct the Antenna Pointing Subsystem (APS).

The DSS Monitor and Control Subsystem (DMC) sends control and configuration information to the DVS from data received from NOCC.

It also collects various calibration and configuration data which are provided to the DVS for logging and transmission, via the GCF, with the VLBI data or separately for monitoring purposes.

At NOCC, the data are displayed in the Network Operations Control Area (NOCA). The personnel in the NOCA use the data for real-time monitoring of VLBI operations. The NOCA also provides the control information to the DSSs, via the GCF, to the DMC.

The NOCC VLBI Processor Subsystem (VPS) performs the cross-correlation of the data from the observing stations and, with further postcorrelation and estimation processing, VLBI information is made available to the user.

The following are the VLBI Processing Subsystem functions:

1. Receives the VLBI and ancillary data via WBDL. An accountability record is made and automatic replay request messages generated to provide the required missing data.

   The ancillary data are used with the accountability data to edit the VLBI data for cross-correlation.

2. Selects correlation rates to ensure that the correlation process can handle the data acquisition without backlog. It is highly desirable to have the correlation process run equal to or faster than WBDL rates.

3. During correlation, the Correlator Assembly generates (with a local model) calibration tones and corrects for phase changes due to drifts in the DVS.

4. Generates the geometric delay and phase and sends the data to the hardware correlator. Due to quantization and round-off, the hardware may not exactly track the software. However, the error is less than 10^{-4} cycles of fringe.

5. Given a set of parameters, the software model calculates the phase to within 10^{-5} cycles of fringe. Also, a record of the calculations, along with their results, is kept with a precision of 10^{-5} cycles of fringe.

6. Constantly updates the software model's computation of the required geometric delay lag due to the earth's rotation. Eight instantaneous lags (four preceding and four following the nominal geometric delay) are provided to determine the actual geometric delay. The maximum equivalent error of the VPS in tracking the model delay (the error in keeping constant the point of maximum correlation) is 0.01 lag.

7. Requires the following postcorrelation functions for ΔDOR:

   a. Receive spacecraft predicts tape from project navigation.

   b. Compute quasar and spacecraft phase.

   c. Compute VLBI time delay for the quasar and spacecraft.

   d. Provide quasar and spacecraft delay tape to project navigation.

8. Requires the following postcorrelation functions for time and time rate, UT1, and polar motion:

   a. Compute quasar and tone phase.

   b. Calibrate quasar phase for station instrument errors.

   c. Compute calibrated quasar delay.

   d. Resolve cycle ambiguities.

   e. Compute preliminary clock parameters.

f. Calibrate for transmission media effects.

g. Solve for time and time rate, UT1, and polar motion.

h. Provide solved-for parameters to project navigation after validation.

D. VLBI SYSTEM ACCURACY

The Galileo ΔDOR requirement of 50 nanoradians in angular position and a few picoradians in angular velocity corresponds to ΔDOR measurement accuracies of 22 cm for multiple-channel utilization with a span bandwidth of 38 MHz, and 20 to 30 micrometers per second (or slightly less than one mHz at X) for single-channel (narrow band) utilization on DSN baselines. Experience gained from conventional applications of VLBI and results of error analyses indicate that these accuracies should be achievable with the VLBI System. A brief discussion of the major error sources follows (Hildebrand et al., 1982).

1. Signal-to-Noise (SNR)

With proper spacecraft transmitter design, the measurement uncertainty from system thermal noise will depend upon EGRS correlated flux. Although the EGRS Signal-to-Noise Ratio (SNR) can be improved by increasing the channel bandwidth and/or the observing time, both of these options also increase the quantity of data which must be recorded and transmitted to a central site for processing. For the VLBI System, the channel bandwidths are 250 kHz, and ΔDOR observation times will be limited to about ten minutes per source. Consequently, radio sources with correlated fluxes of a few tenths of a Jansky or larger are required. Extrapolations of limited survey data indicate that this should not be a serious constraint if spacecraft-to-EGRS separations of up to ten degrees are acceptable.

2. Clock

ΔDOR measurements are unaffected by a constant time offset between station clocks. A frequency offset will cause an error in multiple channel, wide span bandwidth data corresponding to the clock drift between the spacecraft and EGRS observations. Frequency offsets are typically about one part in 10^{12}, yielding a 30 cm error for a 1000 second time period. With hydrogen maser frequency standards, this can be reduced to less than 10 cm by obtaining an estimate of the frequency offset from the EGRS phase rate. In this case, and for single-channel data, frequency stabilities of a few parts in 10^{14} over ten minutes are required.

3. Instrument

Signal group and phase delays arising in the station hardware are largely common to the spacecraft and EGRS observations and cancel in the difference. However, dispersive phase delays will produce a residual error due to the different character of the two signals. For the current system, this is represented by a two degree RMS phase error in each channel. The resulting error in synthesized delay is controlled to a few centimeters by using signal spanned bandwidths of tens of megahertz.

4. Baseline/UT1/Polar Motion

Imprecise knowledge of the baseline orientation and of UT1 and polar motion parameters causes ΔDOR errors which scale with the offset in hour angle and declination of the spacecraft and EGRS. Overall baseline errors are currently about one meter, but in the future will be maintained below 30 cm by weekly VLBI observations of natural sources.

5. Troposphere

In the orbit determination process, the tropospheric range change is represented by a seasonal model for the refractivity of the wet

and dry troposphere components derived from past radiosonde measurements made at each of the DSN complexes. The total effect at zenith is about two meters. For other elevations the range change is roughly proportional to the path length through the troposphere. The uncertainty in the seasonal model is taken to be four to six centimeters in zenith delay, due mostly to atmospheric water vapor. As this model indicates that complete cancellation of tropospheric delays is achieved if the spacecraft and EGRS are observed at the same elevation angle, independent of azimuth, the effect of horizontal inhomogeneities is also included by introducing an additional zenith uncertainty of one or two centimeters which is uncorrelated between ray paths.

6. Ionosphere

The ionosphere may produce S-band signal delays of the same order as those due to the troposphere, but is much more variable, both temporally and spatially. The error model has a functional dependence on elevation angle, on the angular offset of the ray path from the sub-solar point, and on the uncertainty in the zenith ionosphere at the peak of the diurnal variation. The S-band zenith delay uncertainty can be reduced to less than one meter with the aid of calibrations derived from Faraday rotation data.

For ΔDOR, X-band in conjunction with Faraday calibrations, or simultaneous S- and X-band reception, will probably be required to reliably provide 50 nanoradians angular position accuracy. For single-channel, small scale fluctuations on the order of one S-band cycle in a few hundred seconds are important. As such variations are not well calibrated by Faraday rotation, dual frequencies will be employed for ionospheric calibration.

7. Solar Wind Electron Density

In most geometries a high degree of cancellation of signal delays resulting from charged particles in the solar wind is achieved

with VLBI due to the small separation of the ray paths from the two stations. For ΔDOR, solar wind effects are negligible at X-band if the signal closest approach to the Sun is greater than 50 solar radii. Narrowband fringe rates due to plasma fluctuations are small for closest approach distances larger than 100 solar radii at S-band and 50 solar radii at X-band. Nearer to the sun, dual frequency calibrations are required.

8. EGRS Positions

The positions of individual sources relative to the EGRS reference frame must be known to a level compatible with the desired navigation accuracy. Currently, the JPL catalogue contains approximately 100 compact sources whose position uncertainties are 50 nanoradians or less. Improvements in models and additional observations will yield accuracies of 15 to 25 nanoradians which are required for support of the Galileo mission.

Figure 12 presents the current error sources which root-sum-square (RSS) to the expected error in source position, while Figure 13 presents the various errors which RSS to the expected error in ΔDOR.

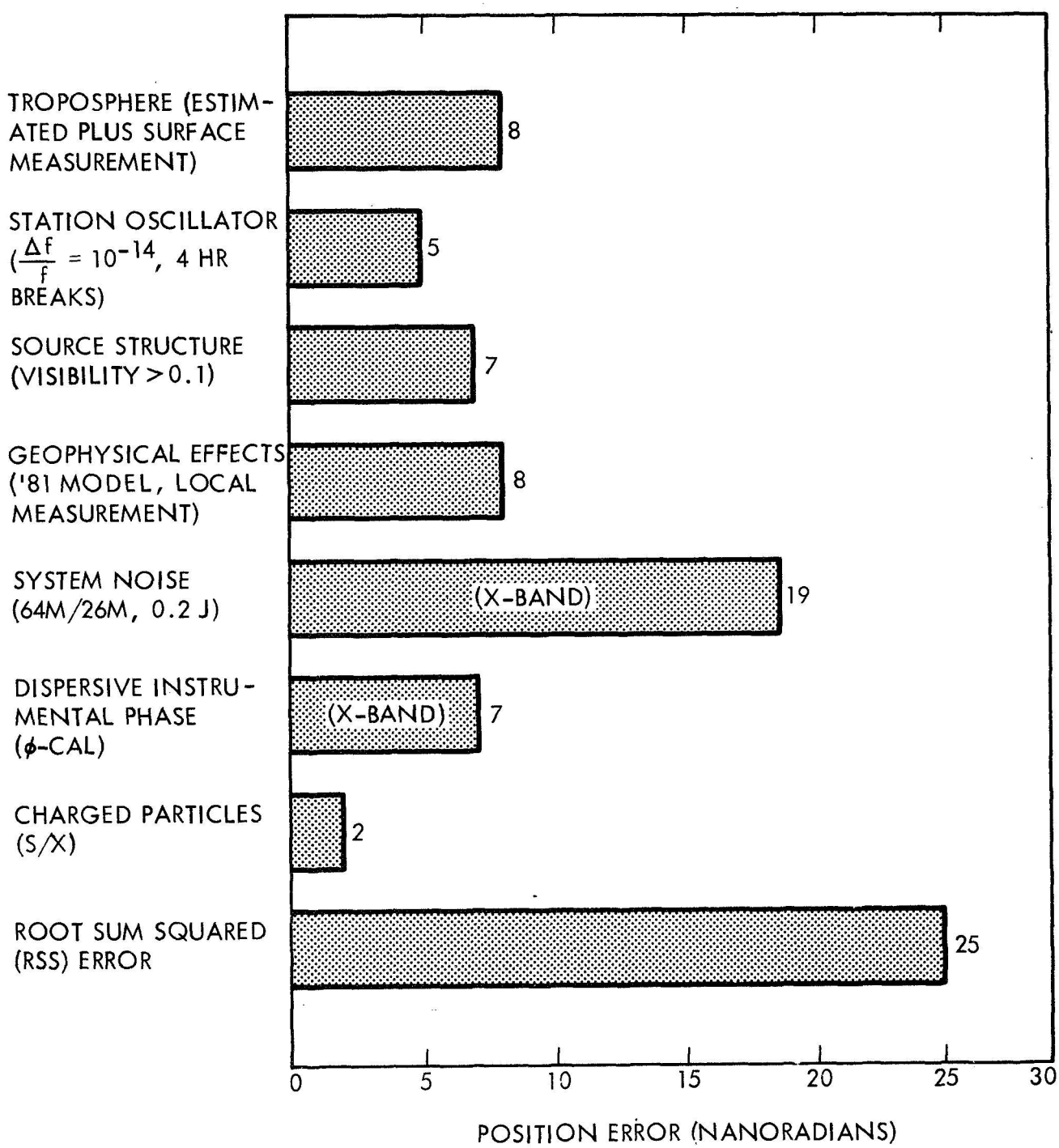

Fig. 12. Expected Uncertainties in Δ DOR Source Positions

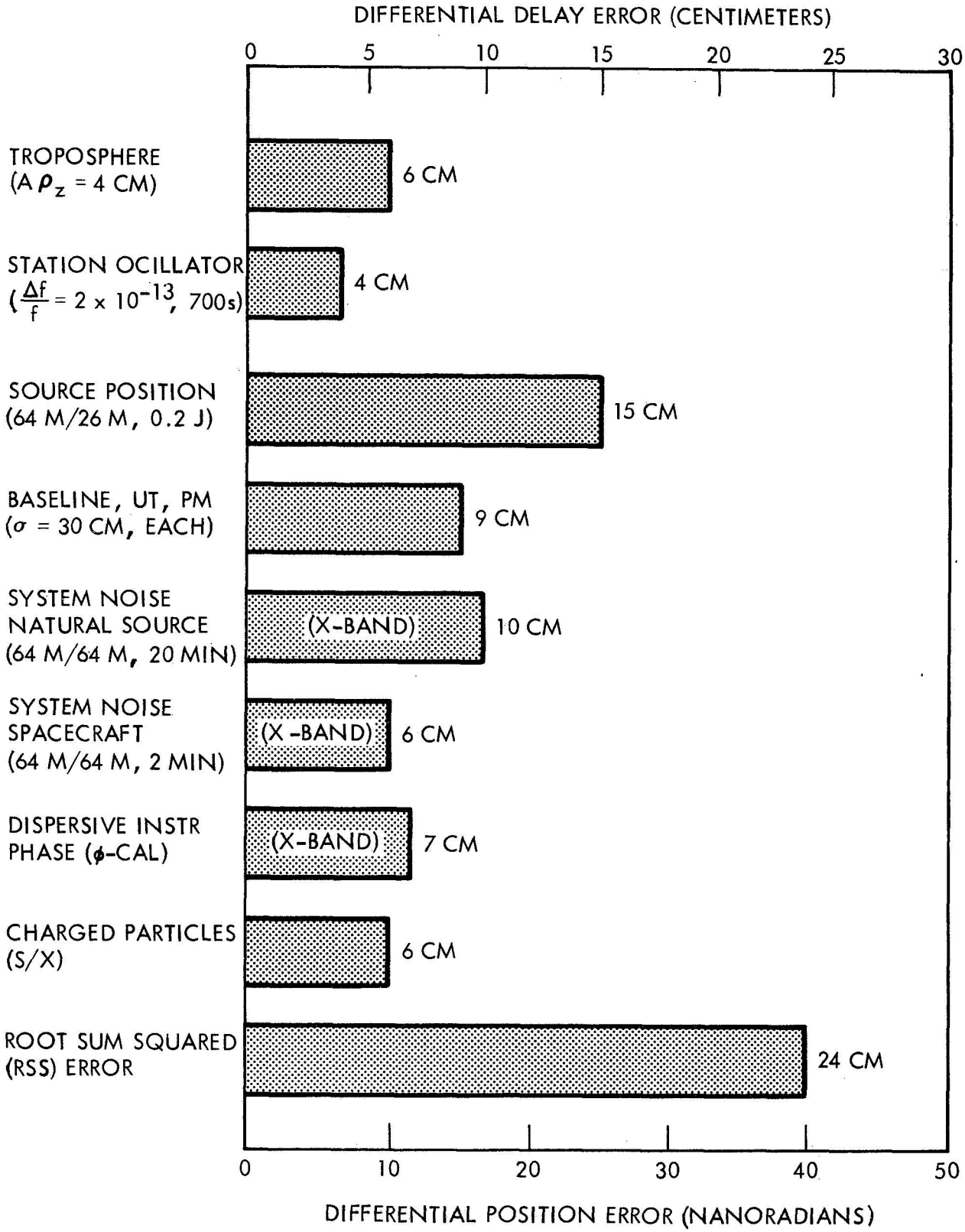

Fig. 13. Expected Error in Δ DOR

IV. DEEP SPACE NAVIGATION

As defined in the introduction, navigation in the NASA planetary program is the process of locating the position and predicted flight path of a space vehicle and correcting that predicted flight path to achieve the mission objectives. The navigation process at the Jet Propulsion Laboratory is carried out by a sequence of actions. First, radio metric data related to the flight path are generated and recorded by the systems described in Parts II and III. These measurements are then processed to determine an orbit or best-estimate trajectory. This orbit determination process is the heart of the entire navigation system. Based on this estimated trajectory and a knowledge of the required targeting or orbit maintenance objectives, trajectory correction maneuver parameters are computed. These parameters, when commanded to the spacecraft and processed by the onboard guidance and control system, result in the execution of trajectory correction thrust maneuvers, which should achieve the desired targeted flight path.

For deep space missions, maneuvers are usually commanded just prior to a critical event such as a planetary encounter, where the target body is to be scientifically observed. The maneuver is, in this case, used to set the flight path on its proper course for meeting the mission goals. Often, the orbit determination process is repeated, after a trajectory correction maneuver, to facilitate accurate science instrument pointing. Then after the encounter, a final best orbit is computed to provide precise reconstruction of the location of the science instrument footprints on the target body.

As we near the end of the second decade of NASA deep space exploration missions, we can look back on a history rich in challenging applications for the radio metric data technologies developed by the Network for navigation. In the 1960's, beginning with the Mariner mission to Venus in 1962, a series of spacecraft were sent to the inner planets to perform remote science sensing during flyby encounters. In the 1970's, the range of navigation applications was expanded to include the delivery of spacecraft to orbit the inner planets; first with the Mariner 9 mission to Mars in 1971, then by the Viking missions to Mars in 1975 and the Pioneer mission to Venus in 1978.

Atmospheric probes to the Venus atmosphere were also delivered by the Pioneer Venus Project. Finally, in the early 1970's, exploration of the outer planets was begun, initially with the Pioneer spacecraft sent to Jupiter and Saturn, and, most recently, with the Voyager spacecraft.

The Voyager mission program, with its two spacecraft sent to both Jupiter and Saturn, including close encounters with some of their natural satellites, represented the most demanding challenge for deep space navigation seen thus far in the NASA planetary program.

Table III details major milestones of the 1970's Missions. Table IV provides the corresponding key events for the actual and proposed deep space missions for the 1980's.

A. THE JPL NAVIGATION SYSTEM

Figure 14 illustrates in schematic form the elements of measurement and computation that comprise the current JPL navigation system, which has been employed for Voyager mission navigation. The left-hand side of the diagram shows a spacecraft acquiring optical TV images of a target body and being tracked by two ground antennas. On the right-hand side is shown the ground processing system, which models the trajectory motion, estimates the orbit, and computes the flight path corrections.

The baseline navigation measurement system of the 1960's consisted of the 2-way S-band (2.3 GHz) doppler, described in Part II, and indeed this system was used to navigate the early Mariner missions to Venus and Mars. Beginning with Mariner 9, 2-way, 1 MHz bandwidth ranging data were also employed. Ranging was used as supplementary data to doppler during the cruise to Mars, and was used as a backup for doppler during the planet orbital phase, when the doppler data noise increased dramatically near superior conjunction.

Ranging data, if generated nearly simultaneously by two widely separated stations on earth, can be used to obtain a direct measurement of the geocentric direction to a spacecraft. Voyager navigation used ranging data acquired in this near-simultaneous mode.

Table III. Major Space Flight Project Milestones in the 1970's

DATE	EVENT
May 30, 1971	Mariner 9 launch
October 12, 1971	Mariner 9 Mars orbit
March 3, 1972	Pioneer 10 launch
April 6, 1973	Pioneer 11 launch
November 3, 1973	Mariner 10 launch
December 4, 1973	Pioneer 10 Jupiter encounter
February 5, 1974	Mariner 10 Venus encounter
March 29, 1974	Mariner 10 Mercury encounter
September 21, 1974	Mariner 10 Mercury encounter
December 3, 1974	Pioneer 11 Jupiter encounter
December 10, 1974	Helios 1 launch
March 15, 1975	Helios 1 first perihelion
March 16, 1975	Mariner 10 Mercury encounter
August 20, 1975	Viking 1 launch
September 9, 1975	Viking 2 launch
January 15, 1976	Helios 2 launch
April 18, 1976	Helios 2 first perihelion
June 19, 1976	Viking 1 Mars orbit insertion
July 20, 1976	Viking 1 Mars landing
August 7, 1976	Viking 2 Mars orbit insertion
September 3, 1976	Viking 2 Mars landing
August 20, 1977	Voyager 2 launch
September 5, 1977	Voyager 1 launch

Table III. Major Space Flight Project Milestones in the 1970's (Cont.)

DATE	EVENT
May 20, 1978	Pioneer-Venus Orbiter launch
August 8, 1978	Pioneer-Venus Multi-probe launch
December 4, 1978	Pioneer-Venus Orbiter orbit insertion
December 9, 1978	Pioneer-Venus Multi-probe atmosphere entry
March 5, 1979	Voyager 1 Jupiter encounter
July 9, 1979	Voyager 2 Jupiter encounter
September 9, 1979	Pioneer 11 Saturn encounter

Table IV. Actual and Anticipated Major Space Flight Project Milestones in the 1980's

November 1980	Voyager 1 Saturn/Titan encounter
August 1981	Voyager 2 Saturn encounter
1984	AMPTE launch
1985	ISEE-3 Giacobini-Zinner Comet encounter
1986	Galileo launch
1986	ISPM launch
1987	Venus Radar Mapper launch
1987	ISPM Jupiter flyby
1988	Galileo Jupiter Probe Atmosphere Entry
1988-90	Galileo Galilean satellite tour
1988	Venus Radar Mapper orbit phase

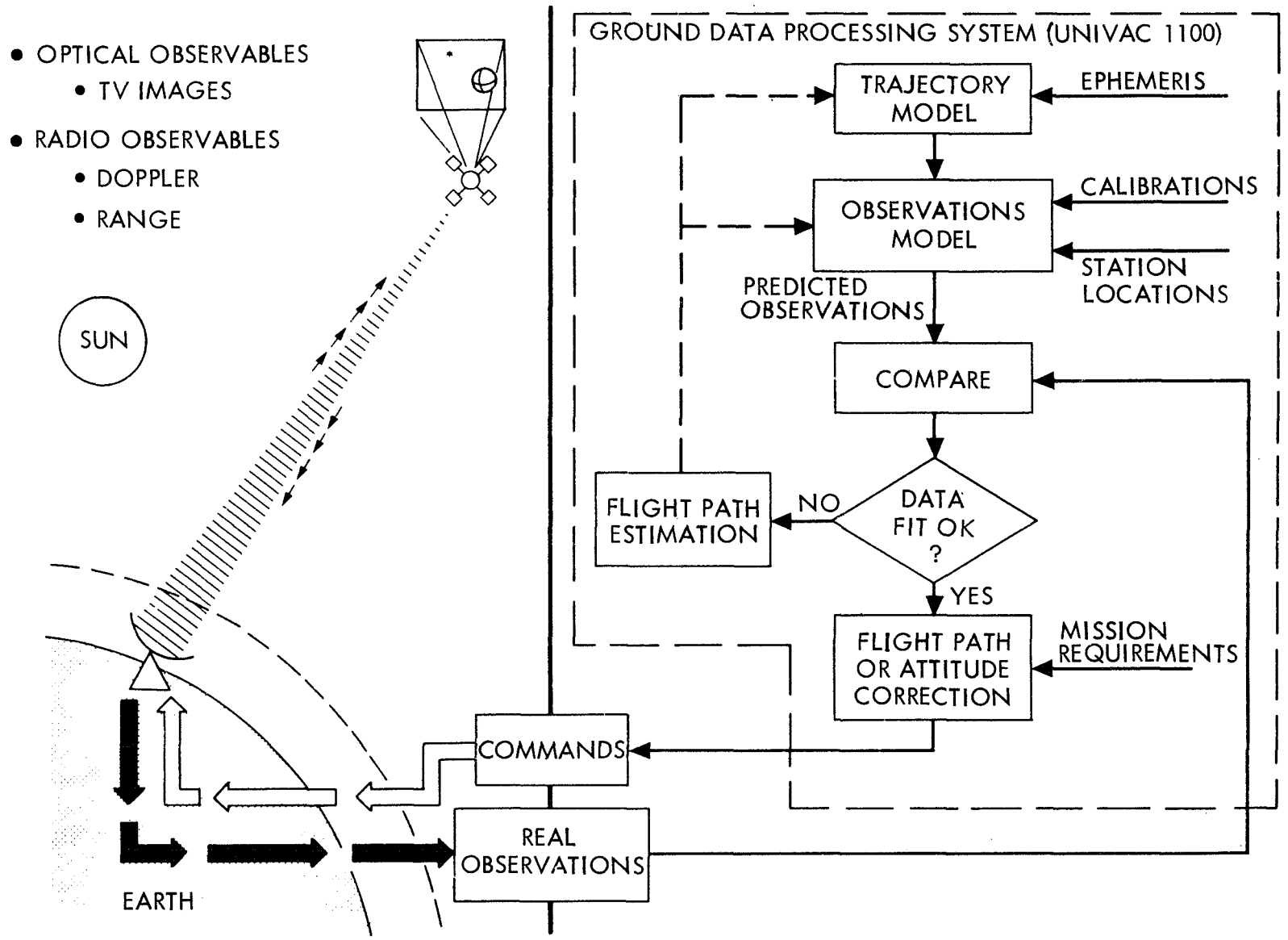

Fig. 14. The JPL Navigation System

Beginning with the Mariner Venus Mercury mission in 1973, NASA spacecraft transponders have transmitted both S-band and X-band (8.4 GHz) downlinks to the earth, with both signals coherent with the uplink S-band. The processing of S- and X-band data allows a calibration of the effects of charged particles on the downlink signal. Mapping methods are employed to infer the effect on the uplink. This dual frequency technique has been used successfully to calibrate both doppler and range during periods of high electrical activity in the solar plasma and earth's atmosphere. It should be noted that optical measurements, acquired from the science TV instruments onboard the spacecraft, have been used on the Viking and Voyager missions to improve the target relative orbit determination accuracies in the final approach stages of their encounters.

Doppler and range data, which are generated by the Deep Space Stations, are brought to the Jet Propulsion Laboratory over high speed data lines and buffered on computer tape within the Tracking System. A large software system is operated within the navigation facility at JPL to determine the spacecraft orbit and compute trajectory correction parameters. The major program segments of this software system are listed in Table V. For each program, the table provides a short function description, the size of the program in terms of the approximate number of lines of FORTRAN code, and the resident computer.

Newly acquired radio metric data are first processed in the navigation facility in the Intermediate Data Records Stripper Processing System (IDRSPS) Program, where the data blocks from different stations are merged into a single time-sequenced array. Any data of poor quality are edited from the array in this system, and the edited data are made ready in computer storage for the orbit estimation process.

Two major modules are used in the orbit estimation process. First is the Double Precision Trajectory (DPTRAJ) system, which computes an N-body numerical integration of the trajectory and state transition partials from initial conditions. The equations are developed in a cartesian frame referenced to the earth's mean equator and equinox of 1950.0. The numerical integration is performed using a variable order predictor-corrector method. The second major module, the Orbit Determination Program (ODP), computes simulated observables corresponding to each actual observation based on the

Table V. Major Software Segments of the JPL Navigation Data Processing System

PROGRAM	FUNCTION	APPROX SIZE (LINES OF FORTRAN CODE)	COMPUTER
ODP	FITS DATA TO OBTAIN ORBIT	200,000	UNIVAC 1100
DPTRAJ	INTEGRATES TRAJECTORY	150,000	UNIVAC 1100
MOPS	COMPUTES CORRECTION MANEUVER	60,000	UNIVAC 1100
IDRSPS	EDITS AND FORMATS RADIO DATA	30,000	UNIVAC 1100
MEDIA	CALIBRATES RADIO DATA	30,000	UNIVAC 1100
ONP	COMPUTES OPTICAL DATA PARTIALS	20,000	UNIVAC 1100
ONIPS	EXTRACTS OPTICAL OBSERVABLES	20,000	MODCOMP IV

trajectory "modeled" by DPTRAJ and computes the partial derivatives of the observables with respect to the initial conditions of the trajectory. It may also compute partial derivatives with respect to a multitude of additional trajectory and observation model parameters, such as planet gravity terms, target ephemeris coordinates, spacecraft gas leaks, and station coordinates. An array of observation residuals is computed and a regression analysis is performed to produce a best estimate of corrections to the initial state parameters and the other desired parameters. The estimation algorithm may, at the user's request, be either batch-least squares or sequential, with stochastic accelerations modeled if desired. The estimation process can be repeated, iteratively, until convergence is obtained. The product of the process is a numerically integrated trajectory which best fits the observations.

This best-estimate trajectory serves as the basis for the computation of the velocity correction parameters required to correct the flight path to meet the mission target objectives. This computation is performed in the Maneuver Operations Program (MOPS).

B. RADIO NAVIGATION ACCURACY

The discussion of navigation accuracy is limited here to the interplanetary phase of space flight and will not include the planet orbiting phase.

Navigation accuracy for interplanetary flight can be defined by the uncertainty with which a spacecraft is delivered to its target. It should be pointed out that the delivery error to a planet or distant satellite is usually comprised almost totally of the target relative orbit determination error. Generally, maneuvers are performed shortly before target encounters, and position errors due to maneuver velocity errors normally do not have time to increase appreciably before the encounter is achieved. It is thus appropriate that we examine the information derived from doppler data received from a station on the Earth tracking a spacecraft in distant space.

The left half of Figure 15 illustrates a station on the earth which is doppler tracking a spacecraft at range ρ, with the earth rotating at rate ω. The doppler signal is proportional to the spacecraft-station range rate, which

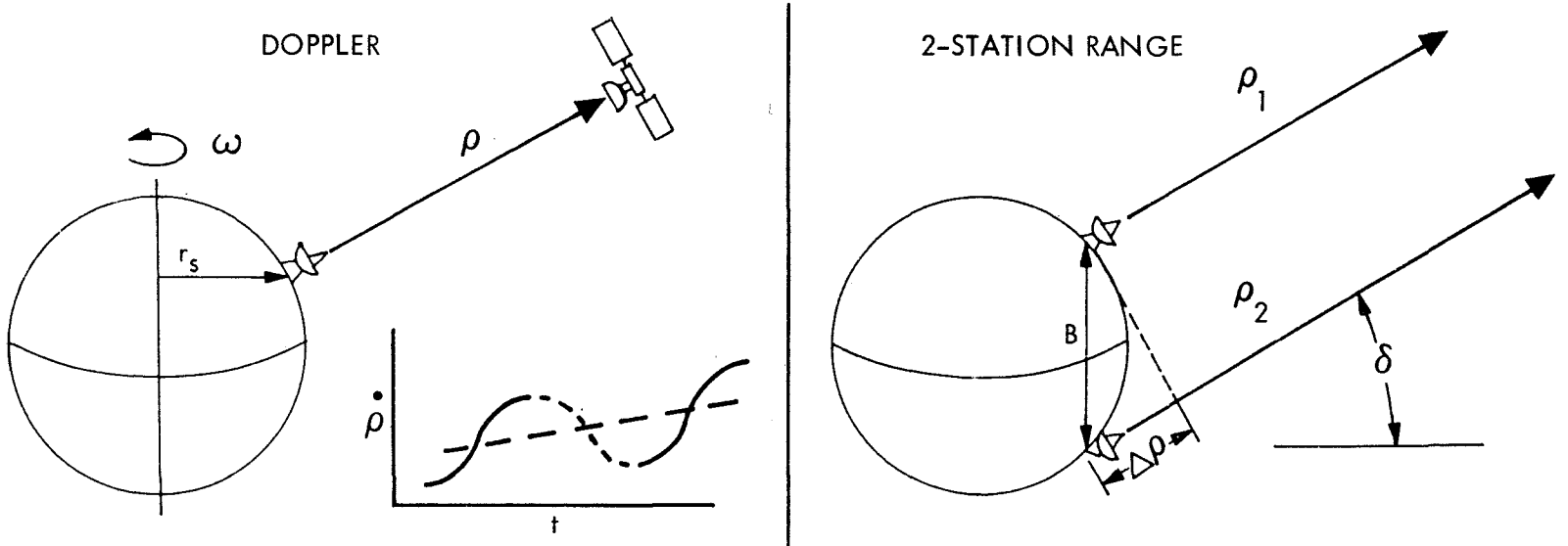

$$\dot{\rho} = \dot{r} + r_s \cos\delta \sin(\omega t + \phi)$$

$$\Delta(\text{AMP}) \sim \Delta(\cos\delta) \sim \sin\delta\,\Delta\delta$$

$$\Delta\delta \sim \frac{1}{\sin\delta}$$

$$\Delta\rho = B \sin\delta$$

$$\Delta(\Delta\rho) = B \cos\delta\,\Delta\delta$$

$$\Delta\delta \sim \frac{1}{\cos\delta}$$

Fig. 15. Earth Doppler Tracking of a Spacecraft

follows in time a pattern which resembles closely a sine wave. From the equation within the figure, it can be seen that the topocentric range rate is approximately equal to the geocentric range rate plus the sinusoidally varying term. The average signal is thus proportional to the geocentric range rate. The phase of the sinusoidal term is proportional to the right ascension of the spacecraft and the amplitude is proportional to the cosine of the spacecraft's geocentric declination. From the equation, it can be seen that the doppler basically measures geocentric angles. It measures right ascension directly and declination through its cosine function. The ability to determine declination, therefore, is inversely related to the sine of the geocentric declination, which explains the traditional low declination problem often referred to in space navigation literature. The accuracy of the determination of right ascension is not particularly sensitive to variations in geometry.

An obvious concern therefore develops if the target planet is near zero declination when encountered by the spacecraft. Conceptually, a singularity occurs and doppler orbit determination accuracies in declination decrease sharply. Since Saturn was at near zero declination when both Voyager spacecraft encountered the planet, a new radio metric data observable, near-simultaneous two-station two-way range, was developed for that mission.

If two stations with a long north-south baseline, as shown on the right half on Figure 15, measure the range at almost the same time, errors in the measured range are proportional to the reciprocal of the cosine of the declination, not the reciprocal of the sine. Hence, no singularity occurs at zero declination. The current planetary ranging system produces deep space range measurements accurate to approximately 5 m, hence two-station range from stations at California and Australia, with a north-south baseline of 5000 km, can provide a direct measurement of a spacecraft declination accurate to about 1 microradian.

Figure 16 illustrates in schematic form the approximate navigation accuracy which is inherent in the current JPL doppler-range navigation system. In the figure a 1 sigma uncertainty in declination is plotted against the spacecraft declination. The performance available with doppler is illustrated by the curved line which approaches a declination error of .25 μrad for high

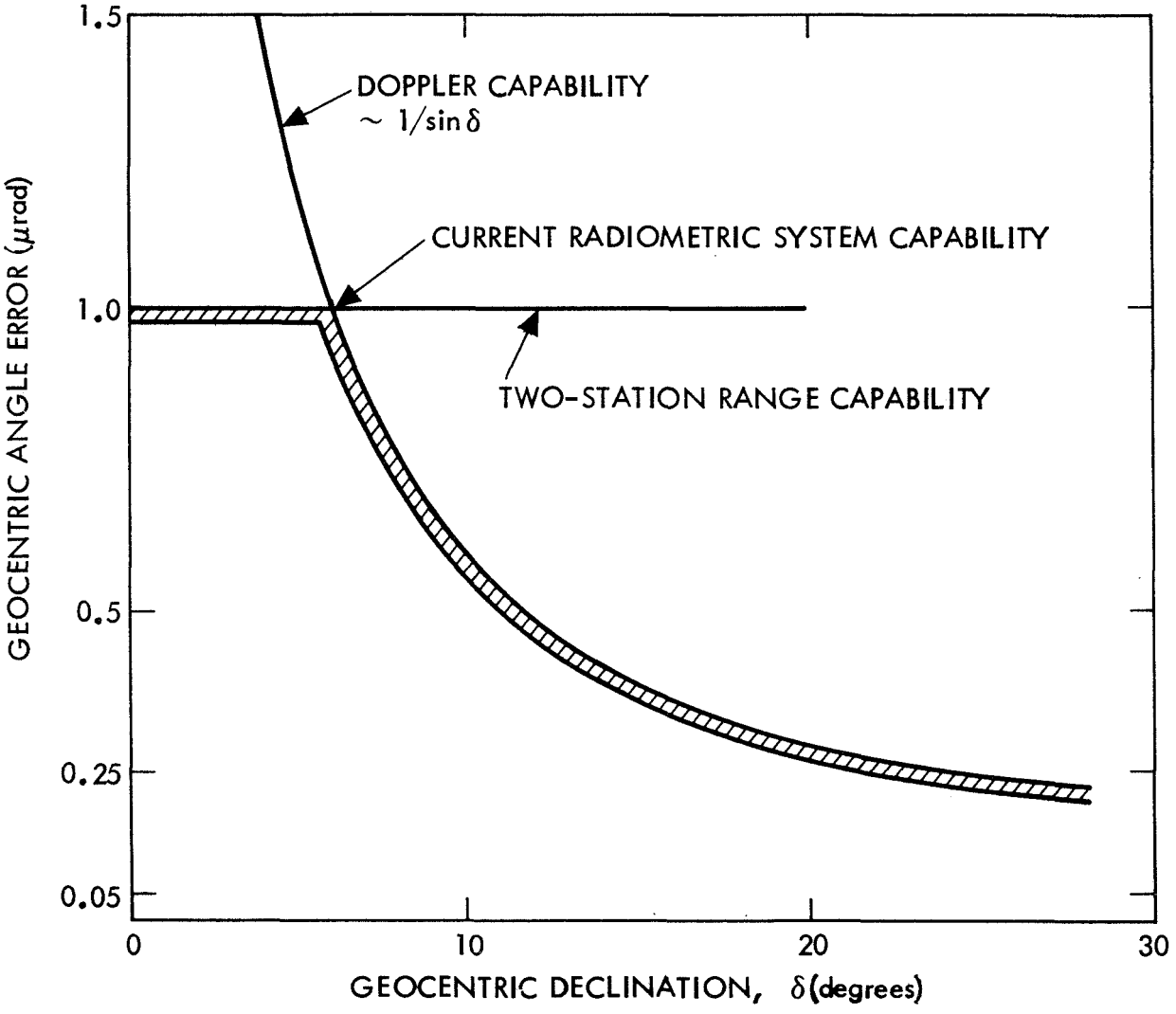

Fig. 16. Navigation Accuracy Capability

declinations but degrades to higher uncertainty for low declinations. The near-simultaneous range measurement provides a one μrad "safety valve" at low declinations. Right ascension, as stated above, is usually determined to within .25 μrad for all geometries.

Achieving the accuracy illustrated in Figure 16 requires precise modelling and computation in the navigation data processing system. Sub-meter observable modelling is employed throughout the navigation processing system, which demands in turn the use of several model support systems to furnish data and constants necessary for accurate computation. Sub-meter modelling is achieved by the use of double precision (18 decimal digits) in all trajectory and observable computations, and the use of a relativistic light time solution algorithm in the doppler and range observable computations. This algorithm takes into account the retardation in the velocity of light by gravity and the transformation from solar system barycentric coordinate time to earth station proper time. Model support systems provide the location of planets and natural satellites in the solar system, the location of the station on the earth, variations in the earth's rotation and orientation, and the effects of transmission media on the radio signal. These are described more fully in Part V.

Figure 16 illustrates typical navigation accuracy performance experienced in the last decade of interplanetary flight. Realized navigation accuracy is, of course, different from mission to mission, depending on the particular mission geometry and often on the number and severity of unusual occurrences during the flight. Factors which influence a "realized" navigation error include: atmospheric disturbances, gas leaks on the spacecraft which erroneously accelerate the spacecraft, and the target location error itself, to name a few. The uncertainty in the ability to model these and other phenomena usually determines the navigation accuracy which is experienced by any particular mission. Table VI lists some of the major "modelling" error sources which affect deep space navigation accuracy. For each error source the table provides a quantitative average estimate of the direct model error and its approximate contribution to the uncertainty in the geocentric direction of a spacecraft.

Table VI. Major Error Sources for Doppler Navigation and Their Effects on Navigation Accuracy

Error Source	Model Accuracy (1982)	Approximate Effect on Geocentric Angle Uncertainty (μrad)
. Station Location on Earth's Crust	1 m	.2
. Ionosphere Charged Particle Effect on Signal Frequency	1 mHz	.2
. Troposphere Neutral Effect on Signal Frequency	.1 mHz	.02
. Station Oscillator Frequency Stability, $\Delta f/f$	1 part in 10^{14}	.003
. Doppler Noise	2 mHz	.02
. Non-Gravitational S/C Forces	10^{-13} k/s^2 (Spacecraft Dependent)	Mission Dependent
. Target Ephemeris (Inner Planets)	10 km/AU	.05
. Target Ephemeris (Outer Planets)	100-200 km/AU	.5-1

C. NAVIGATION OPERATIONS

The navigation system previously described is operated in support of each deep space mission both before and during the actual flight. Long before the actual launch, navigation system software is exercised with simulated data. Error covariances generated in these exercises enable the navigation analyst to identify the effects of the major error sources for the mission of interest, define the total achievable mission accuracy, and determine the required measurements and their acquisition schedule. He also defines performance constraints on the spacecraft systems, such as total required propellant or maximum allowable gas leakage rates. During the flight, the navigation system is operated to support the actual guiding of the flight path. The system produces all of the maneuvers which correct the flight path and furnishes all trajectories used to compute the spacecraft science instrument pointing sequences, tracking antenna pointing, and tuning sequences. Doppler data are processed in the navigation system to investigate all spacecraft anomalies which affect the flight path, such as abnormal gas leaks or impacts with small particles. The navigation system predicts the times of all dynamically related mission events, such as occultation times. Finally, reconstructed navigation orbits are used to accurately locate the instrument viewing footprints, which aid the analysis of the science data.

Operating the navigation system to produce all the required products is a complex and often tedious endeavor. First, a large preparatory effort is required. This includes the setting up of tables and files for over 3000 initialization parameters for the system. These include parameters for the trajectory force models, integration start and end times, options for solution and partial derivative computation, initial state conditions, data filter option, data weighting and calibrations, and options for transforming state vectors and covariances into coordinate systems of interest.

When actual data processing begins, it is conducted as a scientific experiment, in which a hypothesized flight path is adopted and tested against the observations. This testing process usually involves:

1. Computing a multiplicity of flight path solutions including:

    a. Solutions for various radio tracking data arc lengths or constant length data arcs located at different places along the orbit, to examine the distinguishing effect of changing geometry.

    b. Solutions for various choices of data types, such as doppler only, range only, doppler plus range, etc., to examine the degree of compatibility or conflict between data types and establish realistic data weighting policies.

    c. Solutions for various combinations of estimated parameters such as solution for spacecraft state only, state plus solar pressure coefficients, state plus earth station locations, state plus planetary ephemeris, and multiple combinations of these and other parameters, to detect mismodelled phenomena and establish corrected model parameter values.

    d. Solutions using various data filtering algorithms and <u>a priori</u> statisics on estimated parameters, to detect and compensate for stochastic forces acting on the spacecraft.

    e. Solutions using different sets of charged particle data calibration coefficients, to examine the quality and reliability of the different calibration techniques.

    f. Solutions with and without the non-gravitational force models derived from attitude limit-cycle data telemetered to earth, to examine the effectiveness of such models.

2. Computing the expected error covariances of all solutions and their sensitivities to errors in other model parameters which are extremely difficult to estimate from available data.

3. Selecting an adopted "best estimate" flight path solution strategy from an in-depth analysis of the following characteristics of all solutions:

   a. The noise and signatures in the data residuals.

   b. The comparison of the flight path estimates with previous results.

   c. The compatibility of model parameter estimated values with estimated values from other sources.

   d. Comparison of computed error covariances and error sensitivities to unestimated model parameter errors and stochastic phenomena.

4. Exercising the adopted strategy to produce the final "best estimate" flight path.

The computation of maneuvers is also a complex process. It requires both the computation of maneuver times which minimize propellant use and achieve high accuracy, and the precise computation of the velocity corrections necessary to reach the desired target. Maneuver analysis also requires a strong interaction with the mission management and the evolving mission goals and policies.

Auxiliary functions also contribute to the complexity of navigation operations. These can include logging of results in a mission log book and visual charts, storing of data and other records in a computer-based data management system, preparing and presenting of product material to the mission operations management, and coordinating functions with other elements of the mission operations team.

D. THE FUTURE--VERY LONG BASELINE INTERFEROMETRY

As discussed in the introduction, the upcoming Galileo mission requires higher navigation accuracy than that achievable with doppler and range. The Network is therefore developing radio metric data based on Very Long Baseline Interferometry technology. The VLBI observable, defined in Part III, involves the simultaneous tracking of first a spacecraft, then a nearby extragalactic radio source, from two widely separated ground-based stations. Through the correlation processing of the spacecraft data, the difference between the times the two stations receive the same signal can be computed to extreme precision, about 1 nanosecond. If the same correlation process is applied to quasar data, a similar time delay is obtained. Both computed time delays are sensitive in almost the same way to station location relative errors, transmission media errors and station timekeeping errors. If the respective time delays are differenced, the resulting doubly differenced delay is relatively insensitive to these major error sources. Whereas the individual time delays provide information which can yield an angular fix to about .25 μradians, the double differencing technique provides a spacecraft direction angle fix accurate to .05 μradians or better, relative to the observed quasar. If the spacecraft signal is narrowband only, (i.e., a single spacecraft's line-spectra signal phase is measured within a single channel of approximately 250 kHz), or doppler, the VLBI technique can measure only the differenced time delay rate of change, which is proportional to the angular rate of change of the spacecraft's geocentric direction.

Figure 17 illustrates how the VLBI system measures time delay from a wide-bandwidth signal. Figure 18 illustrates the spacecraft's transmitted spectra containing widebandwidth information which will allow the VLBI system to measure time delay. The Galileo mission spacecraft transponder is being outfitted to generate modulated sidebands at S- and X-band. The widest separated sidetone is at 19 MHz for X-band and approximately 4 MHz for S-band.

The process of determining the time delay from these signals with VLBI is achieved by utilizing multiple narrowband channels such as used above for the time delay rate measurement. However the phase of the RF sidetones at the lower and upper 19 MHz signal is measured and when this information is divided by the widebandwidth separation of these tones, i.e., a span bandwidth of

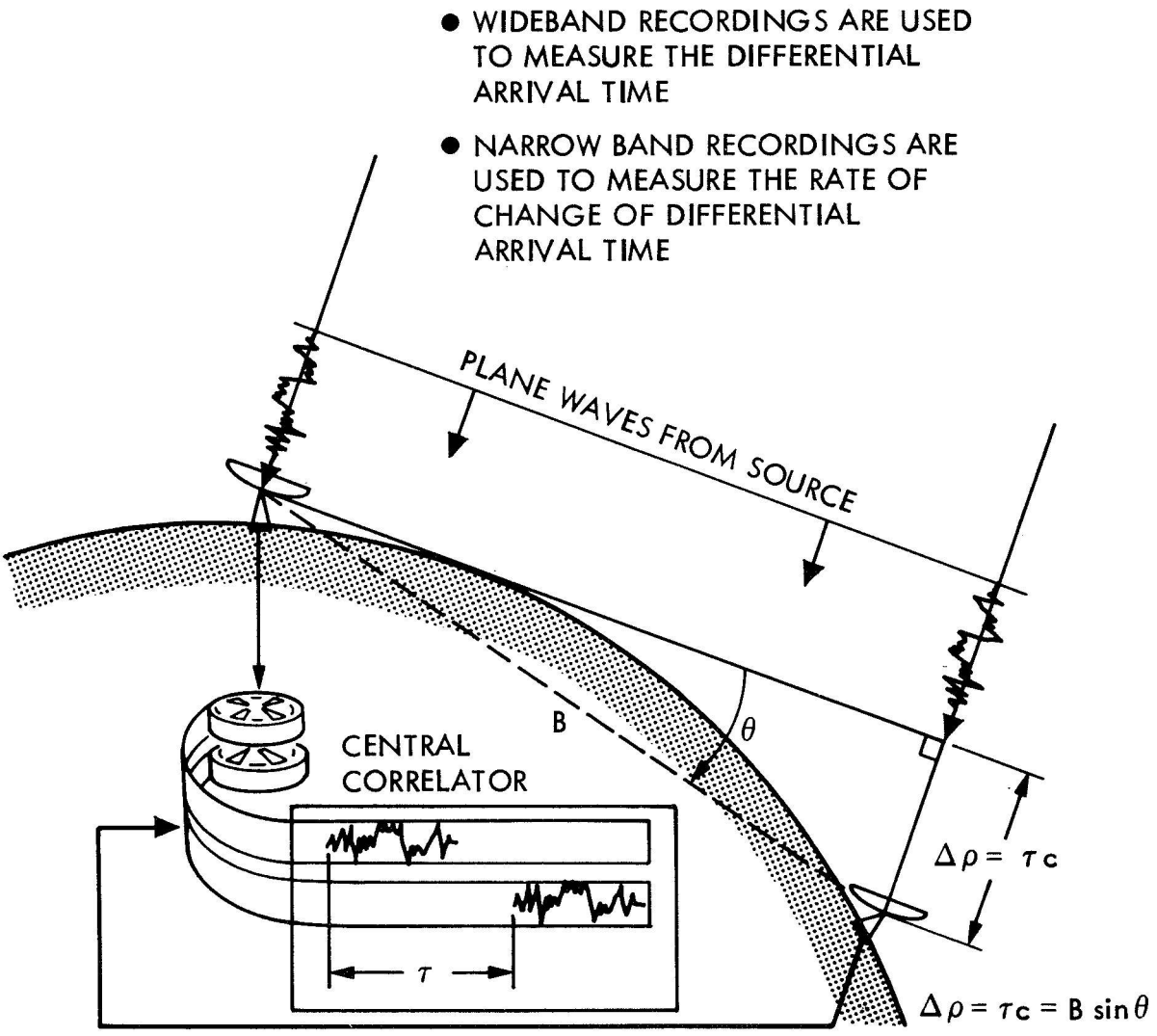

Fig. 17. VLBI System Time Delay

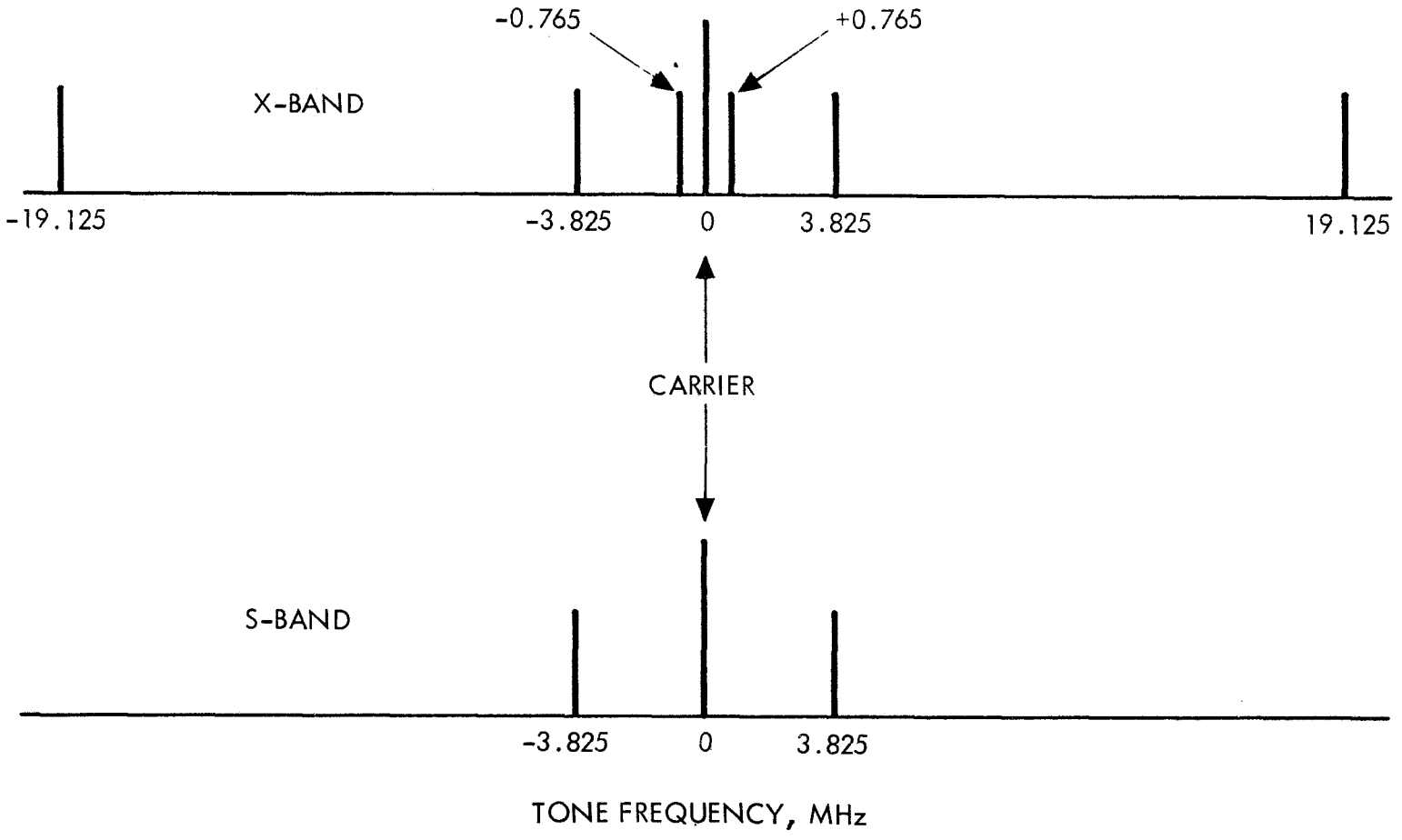

Fig. 18. Galileo Spacecraft Transponder Tones

38 MHz, then the group delay or time delay of the transmitted signal is determined.

The intermediate sidetones between the extreme 19 MHz sidetones serve to resolve the phase ambiguity measurement of the widely separated sidetones. This is the bandwidth synthesis technique of determining the group delay of a wideband signal using only narrowband channels, which provides a bandwidth and data rate processing efficiency.

The combined simultaneous measurement at both S- and X-band is used to help correct the error created by the intervening transmission media.

Widespan bandwidth Δ DOR is thus a downlink doubly differenced range system, which requires only short, 10 minute passes of data, and is accurate to .05 μrad. Its accuracy characteristics are similar to the Voyager system's differenced 2-station, 2-way range in that there is no appreciable degradation at low geocentric declinations, but it is approximately 10 times more accurate. Narrowband VLBI is a doubly differenced one-way doppler system, which also needs only short arcs of data, and can yield geocentric angular rate determination to 5 picoradians/s.

V. NAVIGATION SUPPORT FUNCTIONS

A. TRACKING SYSTEM ANALYTIC CALIBRATIONS (TSAC)

1. Introduction

The primary purpose of the Tracking System Analytic Calibration (TSAC) multimission activity is to estimate physical parameters whose uncertainties limit radio navigational accuracy, and provide corrections ("calibrations") for these effects to the flight project navigation teams. The two principal categories of these error sources are transmission media effects on the radio signal and irregularities in the orientation of the earth. Both categories limit the accuracy of orbits determined from earth-based radio data. Reasons for these limitations will now be discussed.

As was discussed in Section IV, the accuracy of radio metric data depends on the fact that the data contain information about the spacecraft's geocentric direction, i.e., its angular location in the sky. For doppler data, the directional information results from the modulation of the geocentric doppler frequency by the earth's rotation; for near-simultaneous range and wideband VLBI, it results from differential time delay of the signal at two widely separated receiving stations. (See Figure 15, Section IV.) Transmission-media effects influence doppler by introducing systematic variations that resemble the signature of the earth's rotation, and affect range and VLBI by adding additional time delays that differ between the two receiving stations.

Uncertainty in the instantaneous rotation angle of the earth (Universal Time 1 or UT1) and in the direction of the spin axis relative to the earth's crust (polar motion) results in equivalent uncertainty in the instantaneous location of the tracking station. Station-location errors translate directly into angular errors in spacecraft direction; the angular error is approximately equal to the angle subtended by the station coordinate uncertainty at the center of the earth.

2. Transmission Media Effects

Radio signals transmitted from a DSS to a spacecraft and back will pass twice through the earth's troposphere (used here to mean the entire neutral atmosphere) and ionosphere and through whatever solar plasma may be present in interplanetary space along the signal's path. The electromagnetic wave passing through each medium interacts with the electrons in the medium; their motion gives rise to a secondary signal which distorts the main signal in various ways. In the troposphere, where the electrons are bound in atoms, the effect is a frequency-independent reduction in apparent velocity of propagation; group and phase velocities are reduced equally. In the plasmas existing in the ionosphere and in interplanetary space, the electrons are unbound. The resulting frequency-dependent effect is a reduction in group velocity and an equal increase in phase velocity.

Since the troposphere is nearly constant in time, its principal effect on doppler data comes through the change in path length of the air mass along the line of sight as the spacecraft elevation changes during the pass. The ionospheric effect includes the same type of elevation dependence, plus a large diurnal change in total columnar electron content caused by solar ionization during the day followed by recombination at night. Solar plasma effects are much more random over pass length time spans; their longer term magnitude is a function mainly of sun-earth-probe (SEP) angle, becoming large at small SEP angles, when the signal path passes through the regions of high electron density near the sun. The elevation-variation effects of both troposphere and ionosphere have the same period as the earth's rotation, hence introducing systematic errors into the doppler determination of angles.

Troposphere

The total tropospheric one-way range delay varies from about 2.2 m at zenith to 12 m at 10^{o} elevation. The corresponding apparent range rate starts at about -4 mm/sec at 10^{o} as the spacecraft rises; it increases to 0 as the spacecraft crosses the station meridian and to +4 mm/sec at set. The corresponding doppler effect at S-band varies from -60 to

+60 mHz. From the Hamilton-Melbourne equation displayed in Figure 15, the following navigation analyst's rule of thumb may be derived: 1 mHz systematic S-band doppler error is roughly equivalent to 1 meter of station-location error. Current DSS location uncertainties, the limiting error source for doppler, are about 1 meter, so the large tropospheric doppler effects at low elevations must clearly be calibrated. Fortunately, the variability of the zenith tropospheric range delay at a particular station is small, around 5%, and seasonal in nature. The major contributor is the "dry" component, comprising all the dry constituents of the atmosphere. The water-vapor ("wet") portion is small, typically 5% of the total, but contributes most of the variability. A model based on monthly averages of tropospheric parameters at each DSS is used; its estimated uncertainty is about 2% to 3%, corresponding to about 5 cm at zenith, 30 cm at 10^{0} elevation. Zenith range delays are mapped to lower elevation angles in the Orbit Determination Program by interpolation in separate dry and wet tables based on ray-trace results. The tropospheric model is described by Chao (Chao, 1974). Some improvement in this accuracy is sufficient for all missions up to and including the Voyager 2 Saturn encounter. Water-vapor radiometers that measure the wet component of range delay directly along the line of sight will become operational at each DSN complex in 1986. Together with surface barometric-pressure measurements, these radiometers are expected to routinely provide tropospheric corrections accurate to about a centimeter.

Ionosphere

The ionosphere is much more variable than the troposphere. Signal effects are proportional to the integral of electron density along the signal path. This integral, having the dimensions of electrons per unit area, is called total electron content (TEC). In addition to the previously mentioned diurnal TEC variation, which is typically a factor of 5 between day and night, there is a strong dependence of TEC on season and solar cycle. The daily and seasonal time dependence of TEC at Goldstone during 1979, a maximum year in the solar cycle, is shown in Figure 19. A prominent feature of such 3-dimensional plots is the large maximum near each equinox. If the sun-earth-probe geometry is such that the daily

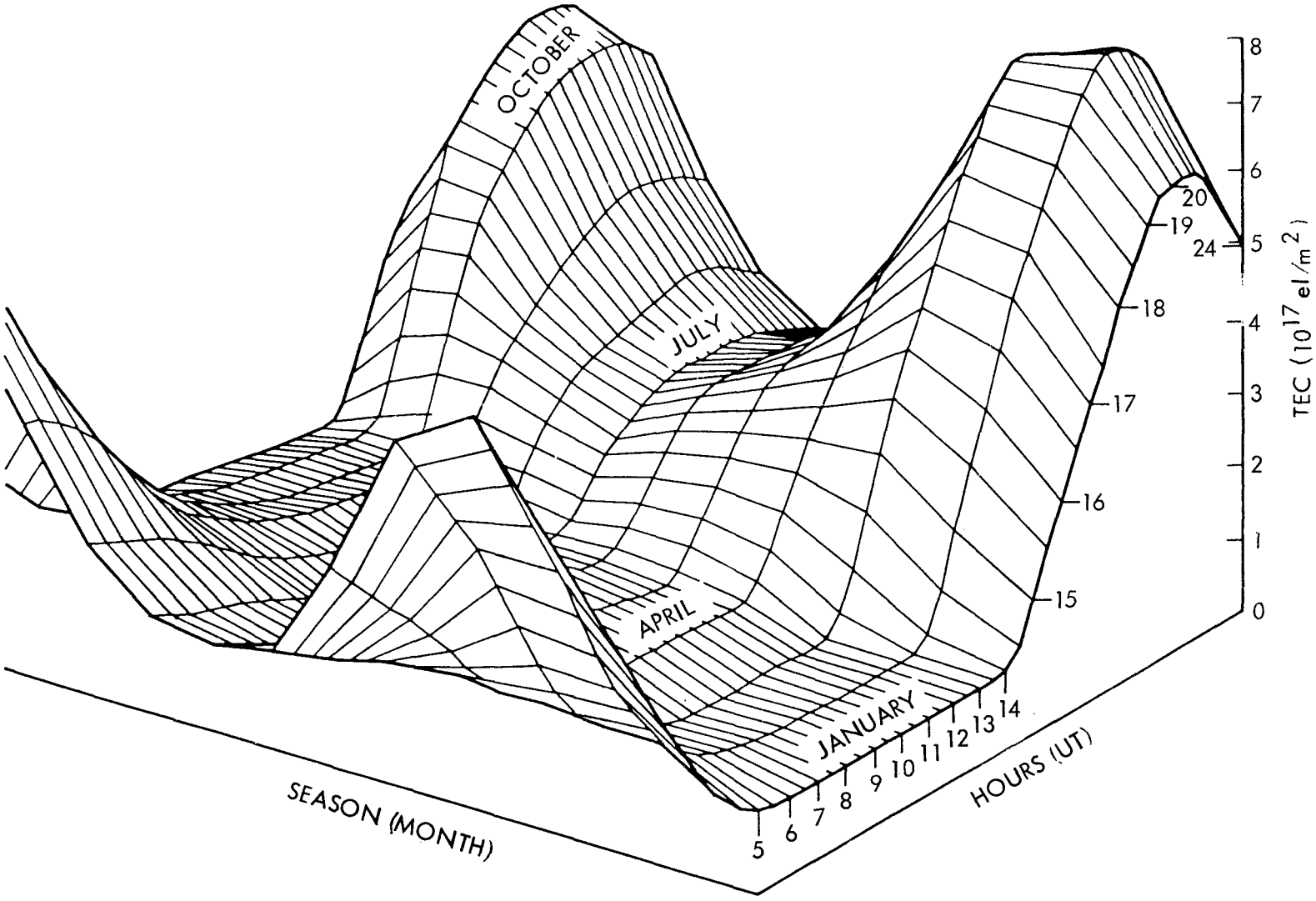

Fig. 19. Daily and Seasonal Time Dependence of TEC

maximum occurs near the start or end of a pass, the combination of that maximum with the longer path lengths at low elevations can result in S-band range delays greater than 20 meters in spring or fall. Some typical ionospheric doppler variations over a pass are +20 to -20 mHz for the elevation effect, 0 to $\pm$ 10 mHz for the diurnal effect. As for the troposphere, these effects are large enough to require calibration. This is done by monitoring TEC along one line of sight at each DSN complex, then mapping that TEC to the varying station-spacecraft line of sight for each pass at each station. The monitoring is carried out by using VHF Faraday-rotation polarimeters pointed at geostationary satellites. Goldstone points at ATS-1 or ATS-5, Canberra at ATS-1 or the Japanese satellite ETS-2, and Madrid at the Italian satellite SIRIO. Faraday rotation refers to the rotation of the plane of polarization of a radio wave passing through a plasma in the presence of a magnetic field, in this case that of the earth. The total rotation is proportional to the integral of the product of electron density and magnetic field component along the path. Knowledge of the magnetic field allows it to be removed from the integral, leaving just TEC. The Faraday data are recorded by the MMA and transmitted weekly to JPL, where they are converted to TEC and stored.

A computer program is used to map this TEC to the spacecraft line of sight and fit the resulting range-delay values with a polynomial that is passed on to the Orbit Determination Program. The uncertainty in the resulting calibration is estimated to be around 1 meter at 10^{o} elevation.

Solar Plasma

The solar wind electron density falls off inversely as the square of the distance from the sun, so that its effects on radio signals are much larger on ray paths passing near the sun, that is, for small sun-earth-probe angles when the spacecraft is beyond the sun. In addition to a steady outflow, plasma events can occur that are many times larger than the normal solar wind. Radio navigation is improved and stabilized if solar plasma is corrected for, but as a rule solar plasma does not pose a serious problem unless it occurs at a critical period when the quantity

of radio metric data is low. Solar plasma effects cancel, to first order, in two-station differenced data such as near-simultaneous range or VLBI. For Voyager, corrections for the effect make use of the dual-frequency (S- and X-bands) downlink doppler data. Because the charged particle doppler shift at X-band is smaller by the square of the frequency ratio, $(3/11)^2$, the line-of-sight downlink TEC can be determined by comparing the two doppler shifts. This TEC will include the net change, since the beginning of the pass, in both solar-plasma and ionospheric downlink electron content. The uplink is inferred from the downlink range delay as a function of time, the mapped ionospheric range delay, and the assumptions that the plasma is concentrated at the point on the ray path nearest the sun and that the spatial electron distribution within the plasma cloud does not change over one round-trip light time between spacecraft and plasma. The validity of these assumptions was established by Wu and Winn (Wu and Winn, 1977). The method is discussed in more detail in a 1980 paper by Green, Lam, and Royden (Green et al, 1980).

3. Earth Orientation Effects

The process of tracking a spacecraft from a DSS results in accurate information on the motion of the spacecraft with respect to the station. For navigation, spacecraft motion relative to the center of the earth is required. It is therefore essential to know where the station is located, at each instant of time, with respect to the center of the earth. This effort is divided into two functions: station location, which is locating each station on the earth's crust, and timing and polar motion, the determination of the orientation of the earth's crust in inertial space. The station location process is discussed in subsection C.

The earth is slowing irregularly; its rotation period with respect to atomic time is long by 2 or 3 ms at present. Furthermore, the earth's principal axis of inertia, determined mainly by the mass distribution of the crust (including the atmosphere and the ocean), wobbles about its spin axis with a period of about 14 months and an amplitude slowly varying between 0 and 10 meters. At DSS latitudes ($\sim 35^{o}$), a 1-ms timing error is equivalent to a DSS longitude error of about 0.4 m, or a right-ascension error of about 0.07 μrad. Polar motion produces periodic

displacements in DSS longitude and spin-axis radius that can be as large as 10 m.

The quantities describing these irregularities are UT1, X, and Y. UT1 can be thought of as the instantaneous angle of rotation of the earth (measured in time units), corrected for polar motion. X and Y are the coordinates of the instantaneous North Pole relative to a conventional origin (fixed on the crust) adopted by international agreement. X is measured toward Greenwich; Y is perpendicular to X, pointing westward. These three quantities thus specify the orientation of the earth in space.

Timing and polar-motion corrections are determined astronomically. The Bureau International de l'Heure (BIH - International Bureau of Time), in Paris, is responsible for keeping and disseminating International Atomic Time (TAI) and civil time, Universal Time Coordinated (UTC). The BIH collects nightly observations from more than 70 observatories throughout the world, analyzes them, and publishes monthly its best estimates of UT1-TAI and the X and Y coordinates of the North Pole. Satellite and VLBI data are also incorporated. In addition, JPL supports the BIH Rapid Service, which obtains data by teletype from about 25 selected observatories, processes it, and sends the results to JPL and other locations weekly by teletype. Every week, TSAC processes both the monthly and Rapid Service data to produce a set of interpolation coefficients for UT1-TAI, X and Y. Each weekly set is valid for a three-year span ending several weeks after the current date.

For times later than the most recent monthly value, standard deviations of the differences between interpolated Rapid Service values and final BIH values (determined later) are typically less than 0.5 m in X or Y and less than 3 ms (1.2 m) in UT1-TAI. The accuracies of the BIH final values are estimated to be of the order of 0.3 m in X or Y, 3 ms in UT1-TAI. VLBI measurements of these quantities using baselines between the three DSN complexes are expected to be significantly more accurate when the TEMPO (Time and Earth Motion Precision Observations; see Subsection F.) system becomes operational in 1983.

B. THE JPL EPHEMERIS PROGRAM

The planetary, lunar, and satellite ephemeris program was begun at JPL in the mid-1960's and has been continuously active since. JPL-produced ephemerides are now the world-wide standard, having been sent upon request to over 150 international users. The program involves the updating and refinement of the ephemerides. This is accomplished by the reduction of a number of different observational data types, least squares fits to these data, and the production of new ephemerides. The process also involves extensive investigations of many types--analytical, dynamical, observational, and numerical.

The quality of the ephemerides depends critically on the types and accuracies of the observational data. Up to the present, the following data sets have been used:

1. Planetary

    a. Optical transit data for the sun and all planets except Pluto, 1911 to present.

    b. Radar-ranging to Mercury, Venus, and Mars, 1967; Mariner 9 spacecraft ranging to Mars, 1971 to 1972.

    c. Viking spacecraft ranging to Mars, 1976; Pioneer and Voyager spacecraft ranging to Jupiter and Saturn, 1979 to 1981.

    d. Satellite photographic positions for Jupiter and Saturn, 1973 to present.

2. Lunar

    a. Laser-ranging to the three Apollo corner reflectors, 1969 to present.

3. Planetary Satellites

   a. Eclipse timings, Galilean satellites, 1878 to 1974.

   b. Occultation timings, Galilean satellites, 1973 to present.

   c. Micrometer measurements, Saturn satellites, 1880 to present.

   d. Photographic positions, Galilean and Saturn satellites, 1947 to present.

At present, the most accurate part of the ephemerides is the inner planetary system (Mercury, Venus, Earth, Moon, and Mars). Because of the highly accurate ranging data, the angles between these bodies are generally known to a level of 0".01 or .05 μrad. The outer planet ephemerides become progressively worse: Jupiter, 0".1; Saturn, 0".2; Uranus and Neptune 0".4; and Pluto, 1". Corresponding values for the Galilean and Saturnian satellite systems are about 0".05 and 0".2, respectively.

As part of the continuing support for the JPL navigation facility, there is now a concentration on the improvement of the ephemerides for Uranus and its satellite system in preparation for the 1986 Voyager encounter. Also, in anticipation of the Galileo Mission to Jupiter, the ephemerides of the system of Galilean satellites are being refined and updated. In the future, the Neptune system will be improved for the eventual Voyager encounter at that planet.

C. GEOCENTRIC EARTH-FIXED COORDINATES OF THE DEEP SPACE STATIONS

Statistical solutions for the coordinates of the Deep Space Stations are obtained from doppler data generated at the encounters of spacecraft with the planets. As each spacecraft flies by one of the planets, doppler data provide a means of precisely estimating the spacecraft orbit relative to the encountered planet and also the coordinates of the stations.

The first step is to obtain single-mission solutions by processing planetary encounter data arcs (with lengths varying from about 5-30 days) with the Orbit Determination Program, described in Part IV. For each planetary encounter data arc, the geocentric position of the target planet is obtained from the planetary ephemeris. Fitting to the 2-way doppler data provides a strong individual-mission solution for the spin radii (u) and longitudes (λ) of the tracking stations. This solution is strongly dependent upon the planetary ephemeris used to process the data. The product obtained from fitting an individual planetary encounter data arc is an augmented information array. This array is modified and placed into the station location data base. It is differentially corrected from the planetary ephemeris used to process the data to the data base planetary ephemeris and to standard values of the station coordinates. Also, the rows for the mission-unique parameters (components of the probe state vector, etc.) are removed after adding a priori information for them.

The "common" parameters for all of the data base augmented information arrays are: the station coordinates u, v, and λ(where v is the distance from the earth's equatorial plane, positive north of the equator); Set III orbital element corrections for Mercury, Venus, the earth-moon barycenter, Mars, and Jupiter; and gravitational constants (GM) for Mercury, Venus, the earth and the moon (neither of which is used), Mars, and Jupiter. In obtaining a combined-mission estimate referred to a particular planetary ephemeris, each data base augmented information array is differentially corrected from the data base planetary ephemeris to the planetary ephemeris to which the combined-mission estimate is to be referred.

The differentially corrected augmented information arrays are combined, and a priori intra-complex survey data are added. The resulting combined-mission augmented information array is input to link SOLVE1 of the ODP, which obtains the combined-mission solution or the desired subset of the common parameters of the array. These are the spin radii (u) and longitudes (λ) of the stations and the gravitational constant of Jupiter GM5 (GM6 will be added when the Voyager 1 and 2 Saturn encounter data arcs are added to the data base). The gravitational constants for the inner planets are well determined and the solution is not improved by estimating them. There is no information content in the doppler tracking data for

estimating the v coordinates of the stations; they are determined from a combination of survey and VLBI data.

The computed standard deviations (σ) for individual-mission solutions for spin radii and longitudes vary from 0.3 to 4 meters. The corresponding figures for combined-mission solutions are 0.2 to 0.6 meters. The individual-mission solutions depart from the combined-mission estimates by less than 2.9 m in u and 5.3 m in λ. The combined-mission estimate for a particular planetary ephemeris is accurate to approximately 1 meter (1σ) in spin radius, u, and 2 meters in longitude, λ . These figures apply specifically for solutions obtained from the ten inner-planet data arcs. Solutions which include outer-planet data arcs will be less accurate because the outer-planet ephemerides are currently less accurate than the inner-planet ephemerides (see Section V.B.).

D. SOURCE CATALOG DEVELOPMENT AND STATION LOCATIONS

In applications of radio interferometry, both navigation of interplanetary spacecraft and geodetic measurements rely heavily on an accurate reference frame composed of extragalactic compact radio sources. Voyager's mission to Uranus and Neptune will employ a reference frame with an accuracy of 0.02 arcseconds, while the Galileo Probe mission to Jupiter (launch date, 1986) demands a frame of radio sources whose relative positions are known to approximately 0".003. Geodetic measurements of a 500 km baseline with an accuracy of 1 cm using radio interferometric techniques also require a reference frame whose accuracy is of the order of 0".003. Development of a reference frame by Very Long Baseline Interferometry (VLBI) requires complete coverage of the sky and several observations of each source during the period of mutual visibility for each pair of stations. A catalog of approximately 100 sources is required to establish a radio reference frame that is adequate for both spacecraft navigation and operational measurements of universal time and polar motion. For these reasons the network has been developing, over the past 11 years, a radio reference frame through observations on the long (8,000-10,000 km) baselines within the Network.

1. VLBI Observations

Between August, 1971 and February, 1980, 48 observing sessions were carried out using 8 different antennas on three continents. In this decade-long sequence, delay and/or delay rate observables were measured on two local baselines (at Goldstone, California and at Madrid, Spain), on a transcontinental baseline (California to Massachusetts, USA), and on two intercontinental baselines (Goldstone to Madrid and Goldstone to Canberra). A multiparameter fit has been applied to the entire ensemble of these observables in order to extract astrometric and geophysical parameters, such as source positions, polar motion, universal time, the precession constant, baseline vectors, and solid earth tides.

In the 48 sessions, which ranged in length from 2 to 48 hours, 117 extra-galactic radio sources were observed. Of the 2412 individual observations, 686 were made at S-band only, 368 at X-band only, and the remaining 1358 were dual-frequency. The observations consisted of 2397 measurements of delay rate and 2153 of delay.

There are seven categories of modeled and adjusted parameters: station locations, tropospheric delays, clock offsets and rates, polar motion and UT1, source positions, the gamma factor of general relativity, and solid-earth-tide parameters. In total, the fit to this span of data includes 765 adjusted parameters.

The software used to perform parameter estimation is based on the square-root-information-filter method (Bierman, 1977) implemented for the VAX 11/780 computer. Approximately 9 CPU hours are required for a solution, with the resultant rms residuals being 0.5 nsec for delay and 0.3 psec/sec for delay rate.

2. Source Positions

The period of 1980-82 was one of continuing improvements in modeling and parameter estimation software. During this time seven source catalogues were produced by fitting the 1971-80 VLBI data. Each succeeding version represented an improvement in modeling, with concomitant improvements in the quality of the fit as well as in the estimated source position uncertainties.

Figure 20 schematically shows the distribution of radio sources in our current reference frame (JPL 1982-4), along with their formal position errors. Notice that the scale for the errors (shown by the shaded box) is different from the location scale. Several important points about these results should be made. The first is that the sky is fairly uniformly covered above -40 degrees declination. However, the galactic plane contains fewer sources because single-antenna radio surveys have not concentrated on this area in the past, and because there is some degradation of the signals from such radio sources by the intervening galactic medium. In spacecraft navigation, this shortage of sources is most critical at the two points where the galactic plane crosses the ecliptic. Unfortunately, critical phases of the Voyager and Galileo missions occur in each of those two regions. Thus, we will be seeking sources in these two areas in the near future.

In the 1982-4 catalog, the average error is somewhat less than 0".005. Based on internal reproducibility tests, and on comparisons with the results of other VLBI groups, it appears that these formal uncertainties are close to the actual uncertainties, with the qualification that the results are heavily weighted by observations obtained between 1978 and 1980. Thus, any mismodeling of the Earth's motion over time scales much greater than three years may be causing systematic errors to which the system is not yet sensitive. Slight mismodeling of nutation is suspected; this question will be resolved over the next few years, as the span of high-quality data approaches a significant fraction of the 18.6-year nutation period.

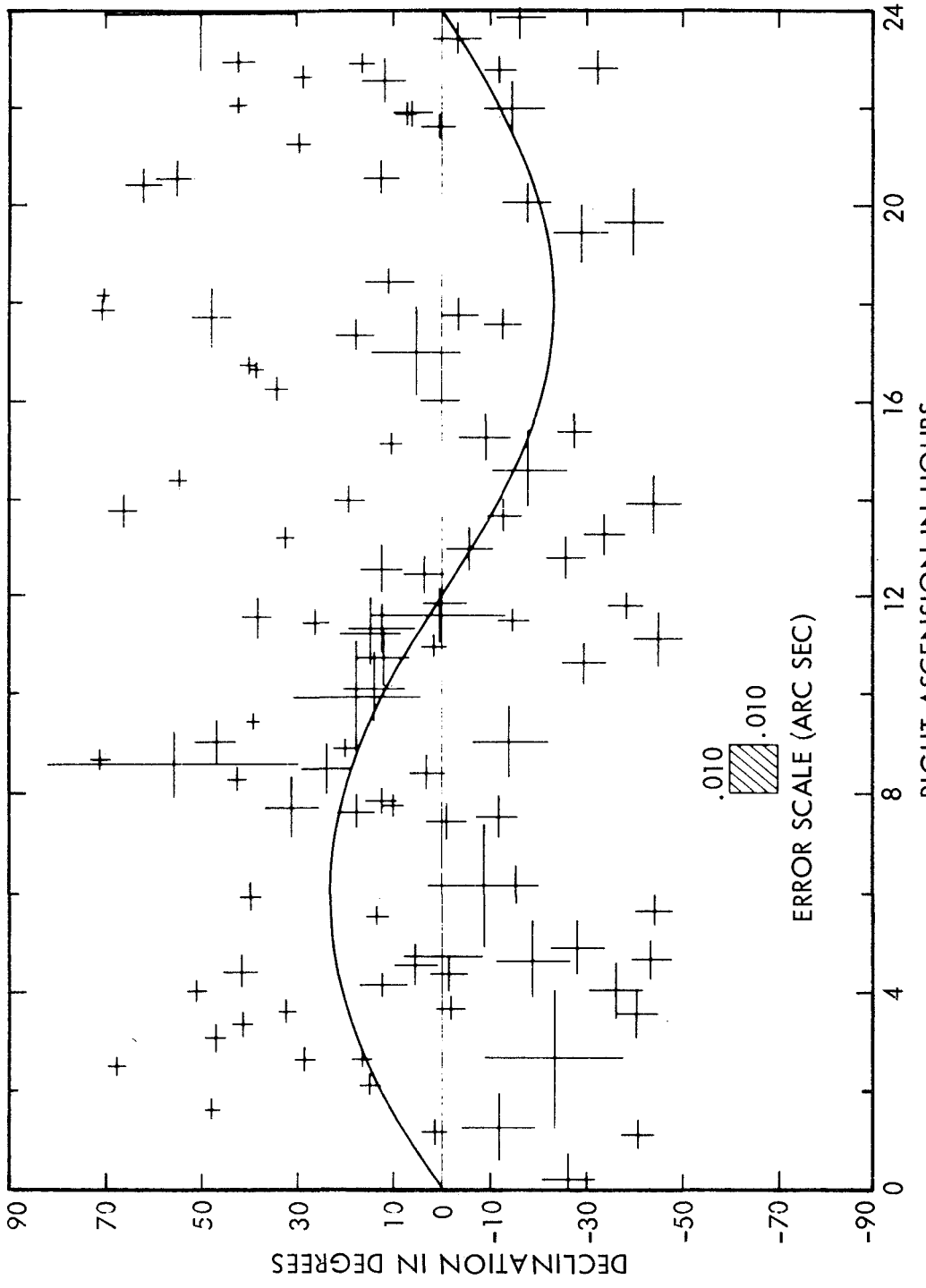

Fig. 20. Schematic Radio Source Positions and Errors for Catalog

Table VII presents the station locations obtained from the standard fit to 1971-80 VLBI data. DSS 14 at Goldstone is the reference station, and the other 7 locations are adjusted. Formal error estimates of the station coordinates range from ~5-6 cm for DSS 13 to ~ 55 cm for the poorly determined equatorial component of Haystack.

E. PLANETARY EPHEMERIS--FRAME TIE

The introduction of ΔVLBI observables as a navigation data type permits spacecraft orbit determination relative to the VLBI reference frame (Newhall, 1982). The origin of this frame, in which the quasar coordinates have been established, is imperfectly known with respect to the planetary dynamical frame. Current estimates of the offset between the two frames are about 0.1 arc second (500 nrad) in right ascension, with declination offset somewhat less, depending on the portion of the celestial sphere being considered.

For encounters, knowledge of quasar and planet positions in a common frame is essential. The Galileo mission requires better than a 50 nrad uncertainty in relative orientation. A four-year program of ΔVLBI observations of the Viking Orbiters and selected angularly nearby quasars produced the first estimate of frame offset: the planetary frame is rotated west of the VLBI frame by 550 $\pm$ 100 nrad in right ascension; the declination offset is less certain: planetary-frame quasar coordinates are 300 $\pm$ 200 nrad greater than their VLBI frame values at 10h right ascension.

Refinement of these results is proceeding, with the use of ΔVLBI observations of Pioneer Venus and additional quasars.

F. VLBI TIME SYNCHRONIZATION AND EARTH MOTION MEASUREMENTS

Spacecraft navigation by two-station differenced ranging techniques requires an accurate knowledge of the time offset between the precision clocks at the two sites (Callahan et al., 1982, and Sovers et al., 1982).

Table VII. Station Locations from 1971-80 VLBI Data

Station	CUD Cylindrical Coordinates					
	Equatorial (m)		Longitude (^{o})		Polar (m)	
DSS 11	5206340.443	0.354	243.1505806	0.0000030	3673764.491	0.173
DSS 13	5215484.859	0.049	243.2051179	0.0000004	3660957.490	0.057
DSS 14*	5203997.735	-	243.1104678	-	3677053.	-
DSS 43	5205251.365	0.104	148.9812791	0.0000011	-3674748.355	0.150
DSS 62	4860817.346	0.196	355.6321629	0.0000028	4116906.653	0.262
DSS 63	4862450.448	0.154	355.7519795	0.0000027	4115109.563	0.242
OVRO	5085449.513	0.103	241.7172840	0.0000011	3838603.800	0.107
HAYST	4700479.590	0.553	288.5118338	0.0000025	4296882.176	0.228

* Reference Station

Knowledge of the clock differences is also useful in monitoring the performance of the clocks. Synchronization of clocks separated by intercontinental distances can be achieved by VLBI in which an extragalactic radio source is simultaneously observed by two radio telescopes. When the two signals are brought to a common site and compared, the apparent difference betwen the arrival times of the signals, as measured with respect to the clocks at the two sites, can be determined. This delay can be used to deduce the clock offset, provided the station locations and the source positions with respect to those stations are known.

To provide the rapid results needed for spacecraft navigation, the Block I VLBI system is being used. Unlike most VLBI systems, which require shipping magnetic data tapes from the stations to a common site, the Block I system allows the received signals to be directly transmitted to the common site (JPL). Although the Block I system can only accommodate a comparatively low data volume, high quality results can still be achieved because of the large antennas and very low noise receivers of the Deep Space Stations. At JPL, the Time and Earth Motion Precision Observations (TEMPO) program conducts weekly measurements of the clock offsets between the Deep Space Network stations using the Block I VLBI system. Figures 21 and 22 show the results of TEMPO measurements of the offset between the timing signals that drive the VLBI equipment at pairs of Deep Space Network sites. The offset is determined with an accuracy of about 1×10^{-7} s. By comparing offsets determined a few days to a few weeks apart, the difference between the rates of the clocks at the two sites can also be determined; the accuracy of this rate difference is about 1×10^{-13} s/s. The VLBI clock synchronization results are consistent with clock offsets determined from LORAN radio broadcasts and from traveling clocks, but are ten times more accurate.

The TEMPO program goals also include rapid determinations of UT1 and Polar Motion (UTPM) to support spacecraft navigation. In order for the program to be a useful UTPM service, it must be able to consistently provide UTPM estimates within at most one month of data acquisition with decimeter or better precision. To support spacecraft navigation, results are needed

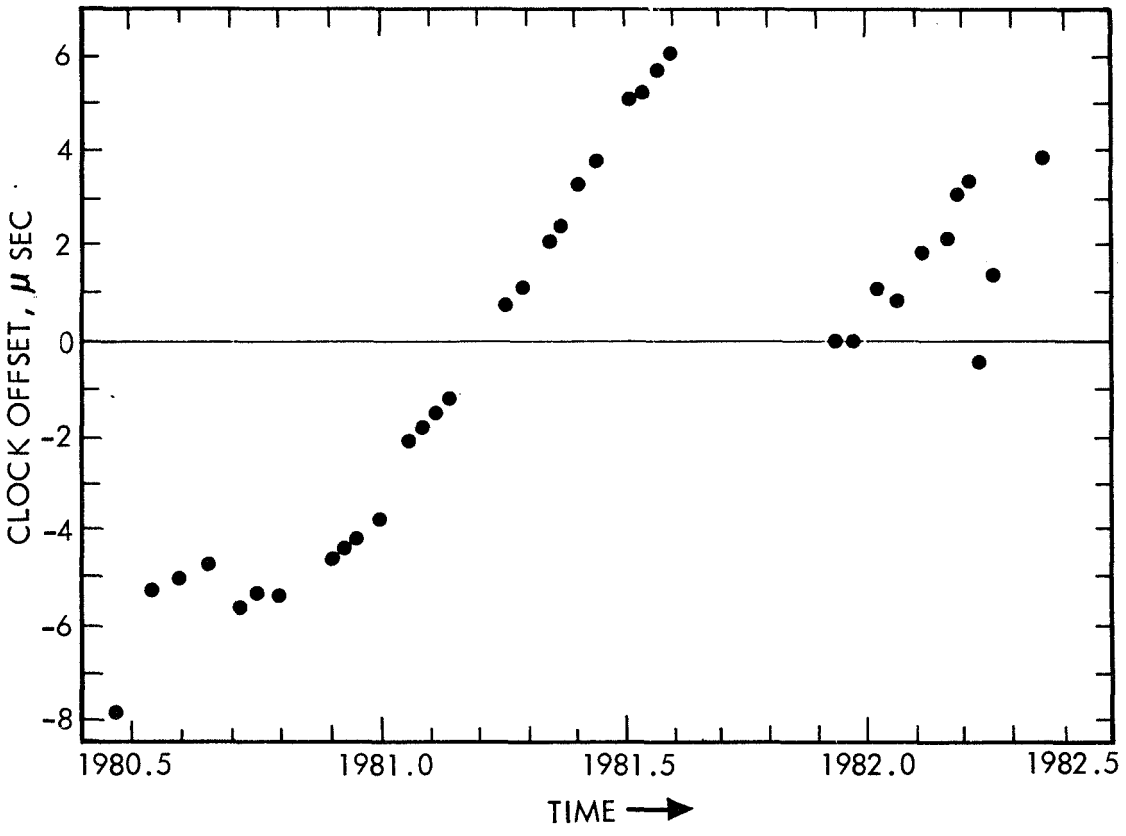

Fig. 21. Clock Offset DSS 43-DSS 14 Determined by the TEMPO Program

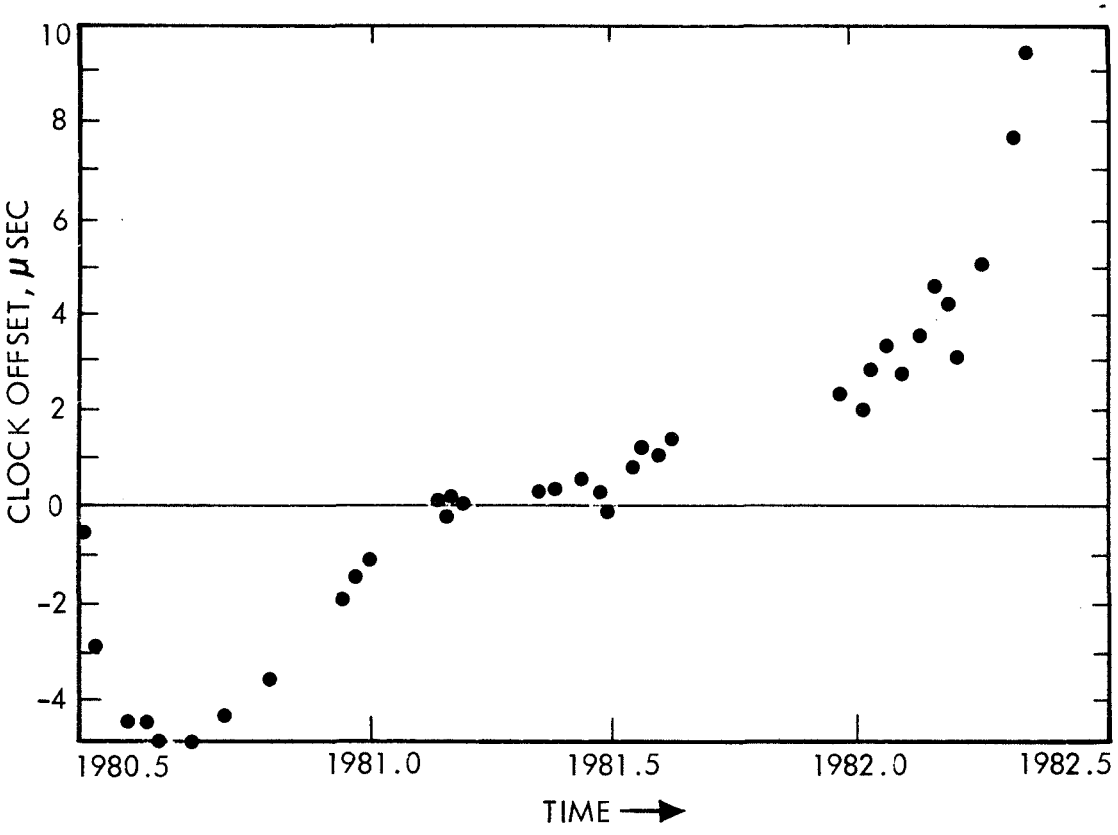

Fig. 22. Clock Offset DSS 63-DSS 14 Determined by the TEMPO Program

within three days of the observations. As of May, 1982, a 22-month history of UTPM had been obtained by the TEMPO program. TEMPO results are consistent with other UTPM estimates and show evidence of UTPM fluctuations on a time scale of a month or less at the decimeter level. By the end of 1983, the TEMPO program should have in place an operational UTPM service both to support JPL navigation efforts and to serve a worldwide user community.

REFERENCES

Bierman, G. J. (1977), "Factorization Methods for Discrete Sequential Estimation," Academic Press.

Callahan, P. S., T. M. Eubanks, M. G. Roth, J. A. Steppe, and P. B. Esposito (1982), "The JPL Near-Real-Time VLBI System and Its Application to Clock Synchronization and Earth Orientation Measurements" to be published in the Proceedings of the International Conference on VLBI Techniques, CNES, Toulouse, France.

Chao, C. C. (1974), "The Tropospheric Calibration Model for Mariner Mars 1971," in TSAC Activities for the MM'71 Mission, pp. 61-76. JPL Technical Report 32-1587, March 1, 1974.

Green, D. W., V. W. Lam, and H. N. Royden (1980), "Effects of the Charged Particle Environment on Voyager Navigation at Jupiter and Saturn." Paper AIAA 80-1650, presented at the AIAA/AAS Astrodynamics Conference, Danvers, Massachusetts.

Hildebrand, C. E., J. S. Border, F. F. Donivan, S. G. Finley, B. Moultine, and L. J. Skjerve (1982), Progress in the Application of VLBI to Interplanetary Navigation, to be published.

Martin, W. L., and A. I. Zygielbaum (1977), "Mu-II Ranging," Technical Memorandum 33-768, Jet Propulsion Laboratory, Pasadena, California.

Molinder, J. I. (1978), "A Tutorial Introduction to Very Long Baseline Interferometry (VLBI) Using Bandwidth Synthesis," in The Deep Space Network Progress Report 42-46, pp. 16-28, Jet Propulsion Laboratory, Pasadena, California.

Newhall, X. X. (1982), "Planetary Frame-VLBI Frame Offsets Derived from Differential VLBI," to be published in The TDA Progress Report 42-72.

Ohlson, J. E., and M. S. Reid (1976), "Conical-Scan Tracking with the 64-m Diameter Antenna at Goldstone," Technical Report 32-1605, Jet Propulsion Laboratory, Pasadena, California.

Otoshi, T. Y. (1975), "A Collection of Articles on S/X-Band Experiment Zero Delay Ranging Tests," Technical Memorandum 33-747, Jet Propulsion Laboratory, Pasadena, California.

Renzetti, N. A., J. P. Fearey, J. R. Hall and B. J. Ostermier (1961), "Radio Tracking Techniques and Performance of the United States Deep Space Instrumentation Facility," in Space Research II, edited by H. C. Van De Holst, C. De Jager, and A. F. Moore, pp. 159-177, North-Holland Publishing Company, Amsterdam.

Renzetti, N. A., and J. P. Fearey (1969), The Deep Space Network, in Space Engineering, edited by G. A. Partel, pp. 559-639, D. Reidel Publishing Company, Dordrecht, Holland.

Renzetti, N. A. (1971), A History of the Deep Space Network from Inception to January 1, 1969, Technical Report 32-1533, Volume 1, Jet Propulsion Laboratory, Pasadena, California.

Renzetti, N. A. and A. L. Berman (1981), The Deep Space Network - An Instrument for Radio Science Research, JPL Publication 80-93, Jet Propulsion Laboratory, Pasadena, California.

Renzetti, N. A. (1982), "Deep Space Network/Flight Project Interface Design Handbook, Document 810-5, Rev. D, Jet Propulsion Laboratory, Pasadena, California (internal document).

Sovers, O. J., J. L. Fanselow, G. H. Purcell, Jr., D. H. Rogstad, and J. B. Thomas (1982), "Determination of Intercontinental Baselines and Earth Orientation Using VLBI," IAG Symposium No. 5, "Geodetic Applications of Radio Interferometry," NOAA Techn. Memo Series, in press.

Spradlin, G. L. (1979), "DSN Tracking System Uplink Frequency Control," in The Deep Space Network Progress Report 42-53, pp. 108-112, Jet Propulsion Laboratory, Pasadena, California.

Spradlin, G. L. (1979), "Deep Space Network System Requirements - DSN Tracking System (1979 through 1983)," Document 821-9, Jet Propulsion Laboratory, Pasadena, California, (internal document).

Thomas, J. B. (1972), "An Analysis of Long Baseline Radio Interferometry," in The Deep Space Network Progress Report, Technical Report 32-1526, Volume VIII, Jet Propulsion Laboratory, Pasadena, California.

Wackley, J. A. (1981), "The DSN Tracking System," in the Telecommunications and Data Acquisition Progress Report 42-63, pp. 8-15, Jet Propulsion Laboratory, Pasadena, California.

Wu, S. C., and F. B. Winn (1977), "A Technique to Determine Uplink Range Calibration Due to Charged Particles," in the Deep Space Network Progress Report 42-41, pp. 57-81.

ABBREVIATIONS

AMPTE	Active Magnetospheric Particle Tracer Explorers
AES	Advanced Equipment Subsystem
AGC	Automatic Gain Control
ANT	Antenna Mechanical Subsystem
APS	Antenna Pointing Subsystem
ATS	Applications Technology Satellite
AU	Astronomic Unit
AUXOSC	Auxillary Oscillator
AZ	Azimuth Angle
BW	Bandwidth
BWS	Bandwidth Synthesis
CCT	Central Communications Terminal
cm	centimeter
CMF	Communication Monitor and Formatter
CPU	Central Processor Unit
CRG	Coherent Reference Generator
dB	decibel
DCO	Digitally Controlled Oscillator
DEC	Declination Angle
DIS	Digital Instrumentation Assembly
DMC	DSS Monitor and Control Subsystem
ΔDOR	delta differential One-Way Range
DPTRAJ	Double Precision Trajectory System
DRG	Data Records Generator
DSN	Deep Space Network
DSS	Deep Space Station
DSCC	Deep Space Communications Complex
DTK	DSS Tracking Subsystem
DTV	Digital Television
El	Elevation Angle
ECS	Error Correction and Switching Assembly
EGRS	Extra Galactic Radio Source

ABBREVIATIONS (CONTINUED)

ETS-2	Engineering Test Satellite 2 (Japan)
FAC	Technical Facilities Subsystem
FTS	Frequency and Timing Subsystem
GCF	Ground Communications Facility
GHz	Gigahertz
HA	Hour Angle
HSDL	High Speed Data Line
Hz	Hertz
IDR	Intermediate Data Record
IF	Intermediate Frequency
ISPM	International Solar Polar Mission
JPL	Jet Propulsion Laboratory
K	Degrees Kelvin
k	one thousand
km	kilometer
kw	kilowatt
LORAN	Long Range Aid to Navigation
m	meter
MDA	Metric Data Assembly
MHz	Megahertz
mHz	Millihertz
MMA	Meteorological Monitor Assembly
MOPS	Maneuver Operations Program
NASA	National Aeronautics and Space Administration
NCB	Narrow Channel Bandwidth
NDPA	Network Data Processing Area
NDPT	Network Data Processing Terminal
NDS	NOCC Display Subsystem
NOCA	Network Operations Control Area
NOCC	Network Operations Control Center
nrad	nanoradians
NRS	NOCC Radio Science Subsystem
NSC	Network Support Controller Assembly
NSS	NOCC Support Subsystem

ABBREVIATIONS (CONTINUED)

NTK	NOCC Tracking Subsystem
ODA	Occultation Data Assembly
ODR	Original Data Record
ODP	Orbit Determination Program
PET	Probe Ephemeris Tape
POCA	Programmable Oscillator Control Assembly
pps	pulses per second
PRA	Planetary Ranging Assembly
RDA	Ranging Demodulator Assembly
RF	Radio Frequency
RSS	Root-Sum-Square
RTM	Real-Time Monitor Assembly
RTLT	Round-Trip-Light-Time
RU	Range Unit (approximately 0.14 m)
s	second
SIRIO	Italian geostationary satellite
SOE	Sequence of Events
TEMPO	Time and Earth Motion Precision Observations Program
TSAC	Tracking System Analytic Calibration
TSF	Track Synthesizer Frequency
TWM	Traveling Wave Maser
UT1	Universal Time One
UTPM	Universal Time and Polar Motion
UWV	Antenna Microwave Subsystem
VCO	Voltage Controlled Oscillator
VHF	Very High Frequency
VLBI	Very Long Baseline Interferometry
VPS	VLBI Processor Subsystem
WBDL	Wideband Data Line
WCB	Wide Channel Bandwidth

NASA—JPL—Coml., L.A., Calif.